Chapter 9
Spread Spectrum Techniques

Spread spectrum systems were originally developed for military applications, to provide anti-jam and low probability of intercept communications by spreading a signal over a large frequency band and transmitting it with a low power per unit bandwidth [97, 263, 305]. However, there are important commercial applications as well. Code division multiple access (CDMA) based on spread spectrum technology is used in 3G cellular systems, including WCDMA and cdma2000. It is also used in wireless local area network standards such as IEEE 801.11 (commonly known as WiFi), and wireless personal area networks such as Bluetooth.

Spread spectrum signals have the distinguishing characteristic that the bandwidth used to transmit a message is much greater than the message bandwidth. This band spread is achieved by using a spreading code or pseudo-noise (PN) sequence that is *independent* of the message and is known to the receiver. This independence property means that modulation schemes such as continuous phase modulation with a large modulation index do not qualify as spread spectrum techniques. The receiver uses a synchronized replica of the PN sequence to despread the received signal allowing recovery of the message. The bandwidth expansion does not combat additive white Gaussian noise (AWGN), but the wide-band character of spread spectrum signals can be utilized to mitigate the effects of intentional and non-intentional sources of additive interference and to exploit the inherent diversity that is present in frequency-selective fading channels.

While there are many different types of spread spectrum systems, the two predominant types are direct sequence (DS) spread spectrum and frequency hopped (FH) spread spectrum. DS spread spectrum achieves the band spread by using the PN sequence to introduce rapid phase transitions into the carrier containing the data, while FH spread spectrum achieves the band spread by using the PN sequence to pseudo-randomly hop the carrier frequency throughout a large band. An excellent tutorial treatment of spread spectrum concepts can be found in the books by Simon et al. [305] and Ziemer and Peterson [378]. Some of the early proposals that applied spread spectrum to cellular radio, such as the system proposed by Cooper and Nettleton [76], were based on FH spread spectrum. However, modern 3G cellular systems use DS spread spectrum. As a result, the focus of this chapter is on DS spread spectrum and DS-CDMA.

While it appears that any cellular system can be suitably optimized to yield a competitive spectral efficiency regardless of the multiple-access technique being used, CDMA offers a number of advantages along with some disadvantages. The advantages of CDMA for cellular applications include (1) universal frequency reuse, (2) narrow band interference rejection, (3) inherent multipath diversity in DS spread spectrum, (4) ability to exploit variable rate speech coding, (5) soft hand-off capability, (6) soft capacity limit, and (7) inherent message privacy. The disadvantages of CDMA for cellular applications include (1) stringent power control requirements with DS CDMA, (2) difficulties in determining the base station (BS) power levels for deployments that have cells of differing sizes.

This chapter begins with an introduction to DS and FH spread spectrum in Sect. 9.1. PN sequences are fundamental to all spread spectrum systems and are the subject of Sect. 9.2. A variety of sequences are considered including *m*-sequences, Gold sequences, Kasami sequences, Barker sequences, Walsh-Hadamard sequences, variable length orthogonal codes, and complementary code keying (CCK). The remainder of the chapter concentrates on DS spread spectrum. The power spectral density of DS spread spectrum signals is considered in Sect. 9.3. Section 9.4 considers the bit error rate performance of DS spread spectrum signals in the presence of tone interference. Section 9.5 discusses the performance of point-to-point DS spread spectrum on frequency-selective fading channels and shows how a RAKE receiver can be used to gain multipath diversity. Section 9.6 considers the performance of a CDMA correlator detector in the presence of multiple-access interference. The chapter concludes with a discussion of CDMA multiuser detection techniques in Sect. 9.7, including optimum CDMA multiuser detection, decorrelation detection, and minimum mean square error (MMSE) detection.

G.L. Stüber, *Principles of Mobile Communication*, DOI 10.1007/978-3-319-55615-4_9

9.1 Basic Principles of Spread Spectrum

9.1.1 Direct Sequence Spread Spectrum

A simplified direct sequence (DS) spread spectrum system with QPSK modulation, termed DS/QPSK, is shown in Fig. 9.1. The pseudo-random (PN) sequence generator produces a spreading sequence $\mathbf{a} = \{a_k\}_{k=1}^{N}$, which is actually a deterministic sequence with period N. This spreading sequence is used to generate the spreading waveform

$$a(t) = A \sum_k a_k h_c(t - kT_c), \tag{9.1}$$

where $\mathbf{a} = \{a_k\}_{k=1}^{N}$ is in general a complex-valued spreading sequence such that $a_k \in \{\pm 1 \pm j\}$, T_c is the PN symbol or chip period, and $h_c(t)$ is a real-valued chip amplitude shaping pulse. The energy per chip is

$$E_c = A^2 \sigma_a^2 \int_{-\infty}^{\infty} h_c^2(t)\mathrm{d}t = A^2 \int_{-\infty}^{\infty} h_c^2(t)\mathrm{d}t \tag{9.2}$$

since $\sigma_a^2 = \frac{1}{2}\mathrm{E}[|a_k|^2] = 1$. Notice that spectral control is achieved in the DS spread spectrum waveform by shaping the PN chips rather than the data symbols.

The data symbol sequence $\{x_n\}$ is used to generate the waveform

$$x(t) = \sum_n x_n u_T(t - nT), \tag{9.3}$$

where A is the amplitude, $\mathbf{x} = \{x_n\}$, $x_n \in \{\pm 1/\sqrt{2} \pm j/\sqrt{2}\}$ is the complex QPSK data symbol sequence, and T is the data symbol duration. It is necessary that T be an integer multiple of T_c, and the ratio $\mathrm{G} = T/T_c$ is called the processing gain, defined as the number of PN chips per data symbol. Two categories of spreading codes can be defined according to the relative values of N and G. A short code has $G = N$, so that each data symbol is spread by a full period of the spreading sequence. A long code has $G \ll N$, so that each data symbol is spread by a subsequence of the spreading sequence.

The DS/QPSK complex envelope, obtained by multiplying $a(t)$ and $x(t)$, is

$$\tilde{s}(t) = A \sum_n x_n h_n(t - nT), \tag{9.4}$$

where

$$h_n(t) = \sum_{k=0}^{G-1} a_{nG+k} h_c(t - kT_c). \tag{9.5}$$

The complex spreading operation is illustrated in Fig. 9.2. Notice that the DS/QPSK signal can be thought of as a QPSK signal where the nth data symbol is shaped with the amplitude shaping pulse $h_n(t)$ in (9.5). For short codes $h_n(t)$ is the

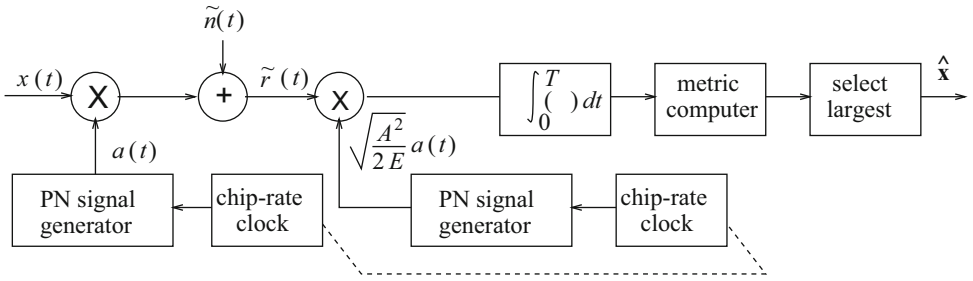

Fig. 9.1 Simplified DS/QPSK system

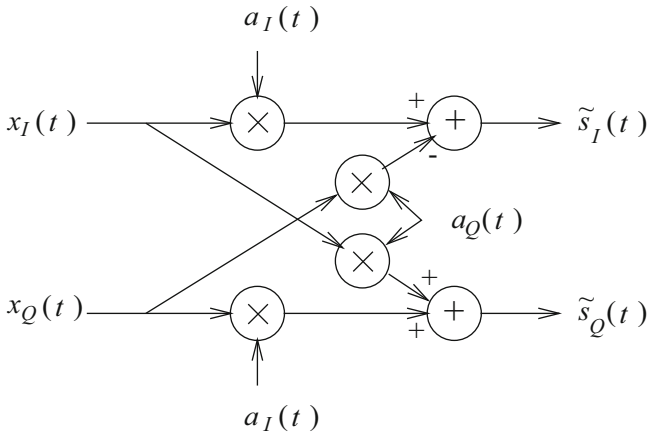

Fig. 9.2 Complex spreading

same for all data symbols. The advantage of complex spreading is a reduction in the peak-to-average ratio of the magnitude of the complex envelope. Offset QPSK (OQPSK) should not be used with complex spreading, since it will increase the peak-to-average ratio. The complex envelope $\tilde{s}(t)$ is applied to a quadrature modulator to produce the bandpass waveform

$$s(t) = A\sum_n \Big(\Big(x_{I,n}h_{I,n}(t-nT) - x_{Q,n}h_{Q,n}(t-nT)\Big)\cos(2\pi f_c t) - \Big(x_{Q,n}h_{I,n}(t-nT) + x_{I,n}h_{Q,n}(t-nT)\Big)\sin(2\pi f_c t)\Big), \tag{9.6}$$

where

$$h_n(t) = h_{I,n}(t) + jh_{Q,n}(t) \tag{9.7}$$

$$x_n = x_{I,n} + jx_{Q,n}. \tag{9.8}$$

During the time interval $[nT, (n+1)T)$, the DS/QPSK complex envelope can assume one of the four possible values

$$\tilde{s}_i(t) = Ah_n(t)x_i\,, \quad i = 1, \ldots, 4. \tag{9.9}$$

Using the basis function

$$\phi_n(t) = \sqrt{\frac{A^2}{2E}}h_n(t), \tag{9.10}$$

where $E = GE_c$ is the symbol energy, gives

$$\tilde{s}_i(t) = \sqrt{2E}x_i\phi_n(t), \quad i = 1, \ldots, 4 \tag{9.11}$$

and it follows that the complex DS/QPSK signal vectors are

$$\tilde{s}_i = \sqrt{2E}x_i, \quad i = 1, \ldots, 4. \tag{9.12}$$

Notice that the basis function $\phi_n(t)$ is indexed with the baud epoch n in the case of long spreading codes.

Besides complex spreading, other types of PN spreading can be used. One possibility is dual-channel quaternary spreading as shown in Fig. 9.3. Usually this scheme is used with OQPSK modulation to reduce the peak-to-average ratio of the magnitude of the complex envelope. If only one data sequence is to be transmitted, then either simple binary spreading or balanced quaternary spreading could be used as shown in Fig. 9.4. Balanced quaternary spreading is known to be less sensitive to interference than simple binary spreading.

Fig. 9.3 Dual-channel quaternary spreading

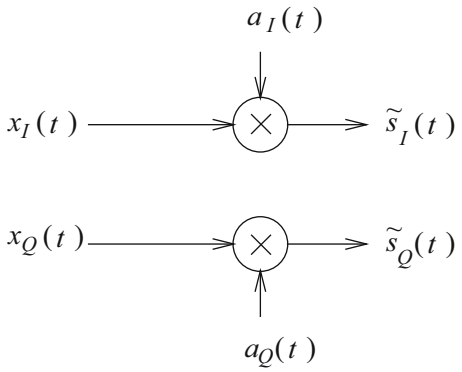

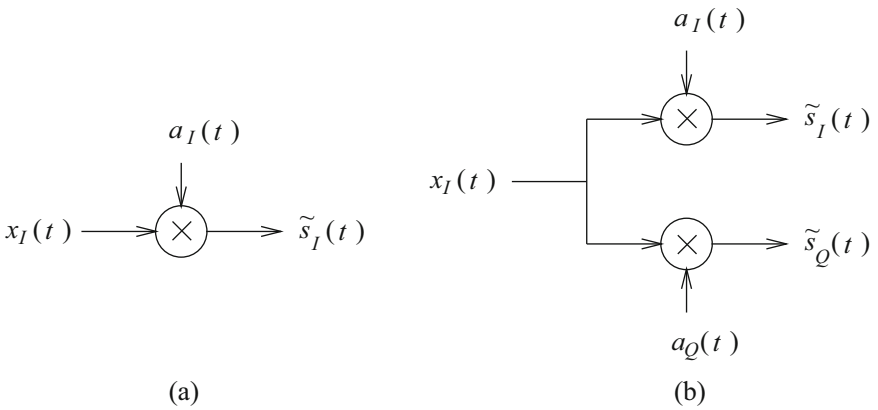

Fig. 9.4 Spreading binary data using (**a**) simple binary spreading, and (**b**) balanced quaternary spreading

Figure 9.1 also shows a simplified DS/QPSK receiver. In general, the DS spread spectrum receiver must perform three functions; synchronize with the incoming spreading sequence, despread the signal, and detect the data. Consider the received complex envelope in the time interval $[nT, (n+1)T)$. This signal can be despread and detected by using the correlator detector in Fig. 5.2 or the matched filter detector in Fig. 5.3, where $\phi_n(t)$ is defined in (9.10). The output of the correlator or matched filter despreader/detector is

$$\tilde{r} = g\tilde{s}_i + \tilde{n}, \tag{9.13}$$

where $\tilde{n}$ is a zero-mean Gaussian random variable with variance $\frac{1}{2}\mathrm{E}[|\tilde{n}|^2] = N_o$.

The ML receiver observes $\tilde{r}$ and decides in favor of the signal vector $\tilde{s}_m$ that minimizes the squared Euclidean distance

$$\mu(\tilde{s}_m) = \|\tilde{r} - g\tilde{s}_m\|^2. \tag{9.14}$$

It follows that the bit error probability of DS/QPSK with Gray coding is identical to that of QPSK, and is given by

$$P_b = Q(\sqrt{2\gamma_b}), \tag{9.15}$$

where $\gamma_b = \alpha^2 E_b/N_o$ is the received bit energy-to-noise ratio. Note that spread spectrum signaling does nothing to improve the error probability performance on an AWGN channel. However, in the sequel spread spectrum signaling will be shown to offer significant error probability performance gains in the presence of additive intentional and non-intentional interference, multipath-fading, and other channel impairments.

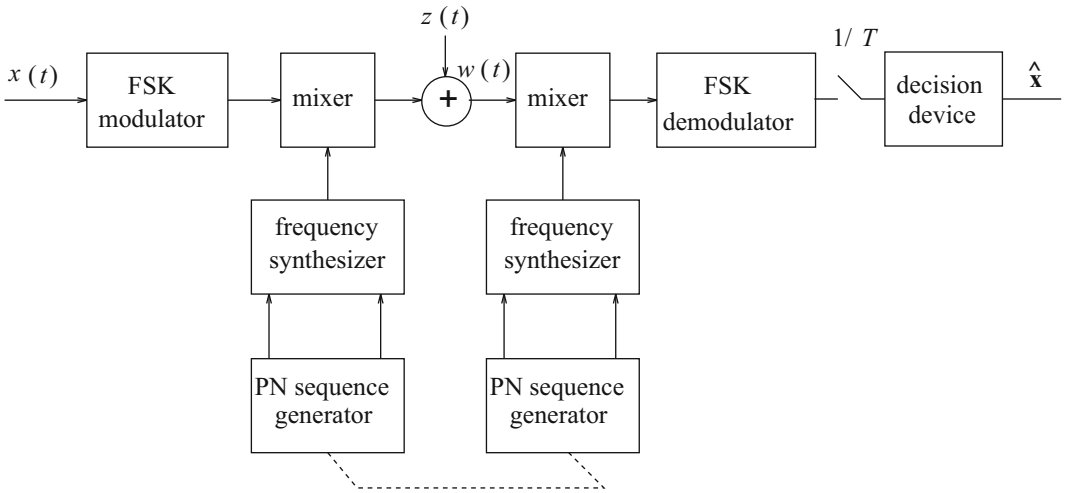

Fig. 9.5 Simplified FH system operating on an AWGN channel

9.1.2 Frequency Hop Spread Spectrum

Frequency hop (FH) spread spectrum systems hop the carrier frequency pseudo-randomly throughout a finite set of hop frequencies. The most common type of modulation with frequency hopping is orthogonal M-ary frequency shift keying (MFSK). The MFSK complex envelope is

$$\tilde{s}(t) = A \sum_n \mathrm{e}^{jx_n \pi \Delta_f t} u_T(t - nT), \tag{9.16}$$

where Δ_f is the frequency separation, and $x_n \in \{\pm 1, \pm 3, \ldots, \pm M - 1\}$. A FH/MFSK waveform can be generated by using a digital frequency synthesizer whose inputs consist of the complex envelope of the modulating waveform $\tilde{s}(t)$ and the contents of a pseudo-noise sequence generator. A conceptual FH/MFSK spread spectrum system is shown in Fig. 9.5.

There are two basic types of FH spread spectrum modulation, fast frequency hopping (FFH) and slow frequency hopping (SFH). SFH systems transmit one or more (in general L) data symbols per hop. The SFH/MFSK complex envelope is

$$\tilde{s}(t) = A \sum_n \sum_{i=1}^{L} \mathrm{e}^{jx_{nL+i} \pi \Delta_f t + 2\pi f_n t} u_T(t - (nL + i)T), \tag{9.17}$$

where the first sum indexes the sequence of hopped carrier frequencies $\{f_n\}$, and the second sum indexes the vector of L data symbols $\mathbf{x}_n = (x_{nL+1}, x_{nL+2}, \ldots, x_{(n+1)L})$ that are transmitted at the nth hop.

FFH systems transmit the same data symbol on multiple (in general L) hopped carrier frequencies. If independent channel conditions are experienced on each of the hop frequencies, then a diversity gain can be achieved by using diversity combining. The FFH/MFSK complex envelope is

$$\tilde{s}(t) = A \sum_n \sum_{i=1}^{L} \mathrm{e}^{jx_n \pi \Delta_f t + 2\pi f_{nL+i} t} u_{T/L}(t - (nL + i)T/L), \tag{9.18}$$

where the first sum indexes the sequence of data symbols, $\{x_n\}$, and the second sum indexes the vector of hop frequencies $\mathbf{f}_n = (f_{nL+1}, f_{nL+2}, \ldots, f_{(n+1)L})$ that are used when transmitting the nth data symbol.

With orthogonal MFSK the required frequency separation Δ_f depends on the type of detection that is used. Coherent detection requires a frequency separation $\Delta_f = 1/2T$, while non-coherent detection requires $\Delta_f = 1/T$ (Problem 4.7). If coherent detection can be used, then the error probability of SFH/MFSK or FFH/MFSK on an AWGN channel is given by (5.119). However, FH/MFSK is often detected non-coherently because of the difficulty in achieving rapid carrier synchronization when the carrier frequency is hopped. The error probability of SFH/MFSK on an AWGN channel with non-coherent square-law detection is given by (5.191). If FFH/MFSK is used on an AWGN channel, then the error probability assumes a more complicated form due to a square-law combining loss [272].

9.2 Spreading Sequences

CDMA systems achieve their multiple-access capability by using sets spreading sequences that are chosen to have three desirable attributes: (1) the sequences are balanced so that each element of the sequence alphabet occurs with equal frequency, (2) the autocorrelations have small off-peak values, to allow for rapid sequence acquisition at the receiver and to minimize self-interference due to multipath, (3) the cross-correlations are small at all delays, to minimize multiple-access interference.

Spreading sequences are often characterized in terms of their discrete-time correlation properties. Let $\mathbf{a}^{(k)} = \{a_n^{(k)}\}$ denote the kth complex spreading sequence.[1] For spread spectrum systems that employ short codes, each data symbol is spread by a full period of the spreading sequence. In this case the full period correlation properties are of interest. The full period autocorrelation of the sequence $\mathbf{a}^{(k)}$ is[2]

$$\phi_{k,k}(n) = \frac{1}{2N}\sum_{i=0}^{N-1} a_i^{(k)^*} a_{i+n}^{(k)} \tag{9.19}$$

and the full period cross-correlation between the sequences $\mathbf{a}^{(k)}$ and $\mathbf{a}^{(m)}$ is

$$\phi_{k,m}(n) = \frac{1}{2N}\sum_{i=0}^{N-1} a_i^{(k)^*} a_{i+n}^{(m)}, \tag{9.20}$$

where N is the length or period of the spreading sequence(s).

The aperiodic autocorrelation of $\mathbf{a}^{(k)}$ is defined as

$$\phi_{k,k}^{a}(n) = \begin{cases} \frac{1}{2N}\sum_{i=1}^{N-n} a_i^{(k)^*} a_{i+n}^{(k)} & , \ 0 \le n \le N-1 \\ \frac{1}{2N}\sum_{i=1}^{N+n} a_i^{(k)} a_{i-n}^{(k)^*} & , \ -N+1 \le n \le 0 \\ 0 & , \ |n| \ge N \end{cases} . \tag{9.21}$$

For spread spectrum systems that employ long codes, each data symbol is spread by only a length-G subsequence of the spreading code. In this case, the partial period correlations are of interest. The partial period auto- and cross-correlations are

$$\phi_{k,k}^{p}(n) = \frac{1}{2G}\sum_{i=0}^{G-1} a_i^{(k)^*} a_{i+n}^{(k)} \tag{9.22}$$

$$\phi_{k,m}^{p}(n) = \frac{1}{2G}\sum_{i=0}^{G-1} a_i^{(k)^*} a_{i+n}^{(m)}. \tag{9.23}$$

The partial period correlations are not only a function of the delay n, but also depend upon the point in the sequence(s) where the summation actually starts. The partial period correlations are difficult to derive analytically, except for certain types of sequences. Therefore, a statistical treatment is often used under the assumption that the sequences are randomly generated, i.e., the sequence elements are chosen randomly from the set $\{\pm 1, \pm j\}$ independently and with equal probability. For random sequences

$$\frac{1}{2}\mathrm{E}[a_n^{(k)}] = 0 \qquad \frac{1}{2}\mathrm{E}[|a_n^{(k)}|^2] = 1 \qquad \frac{1}{2}\mathrm{E}[a_n^{(k)^*} a_n^{(m)}] = 0. \tag{9.24}$$

Hence, the mean value of the partial period autocorrelation is

$$\mu_{\phi_{k,k}^{p}(n)} = \mathrm{E}[\phi_{k,k}^{p}(n)] = \frac{1}{2G}\sum_{i=0}^{G-1} \mathrm{E}[a_i^{(k)^*} a_{i+n}^{(k)}] = \delta_{n,\ell N}, \tag{9.25}$$

[1] The following development also applies to real spreading sequences.

[2] Throughout this section complex spreading sequences are assumed. For real spreading sequences, the correlation functions are similar but are normalized by N rather than $2N$.

where

$$\delta_{n,\ell N} = \begin{cases} 1 \ , & n = \ell N \\ 0 \ , & n \neq \ell N \end{cases} \tag{9.26}$$

and ℓ is an integer. The variance of the partial period autocorrelation is

$$\begin{aligned} \sigma^2_{\phi^p_{k,k}(n)} &= \mathrm{E}[|\phi^p_{k,k}(n)|^2] - \mu^2_{\phi^p_{k,k}(n)} \\ &= \frac{1}{(2G)^2} \sum_{i=0}^{G-1} \sum_{j=0}^{G-1} \mathrm{E}[a_i^{(k)*} a_{i+n}^{(k)} a_j^{(k)*} a_{j+n}^{(k)}] - \mu^2_{\phi^p_{k,k}(n)} \\ &= (1 - \delta_{n,\ell N})(1/G). \end{aligned} \tag{9.27}$$

Likewise, the mean and variance of the partial period cross-correlation are

$$\mu_{\phi^p_{k,m}(n)} = \mathrm{E}[\phi^p_{k,m}(n)] = 0 \ , \quad \forall n \tag{9.28}$$

$$\sigma^2_{\phi^p_{k,m}(n)} = \mathrm{E}[|\phi^p_{k,m}(n)|^2] - \mu^2_{\phi^p_{k,m}(n)} = 1/G \ , \quad \forall n. \tag{9.29}$$

9.2.1 Spreading Waveforms

The full period cross-correlation between two spreading waveforms $a^{(k)}(t)$ and $a^{(m)}(t)$, each of period T, is[3]

$$\begin{aligned} R_{k,m}(\tau) &= \frac{1}{2T} \int_0^T a^{(k)*}(t)\, a^{(m)}(t+\tau) \mathrm{d}t \\ &= \frac{1}{2T} \sum_{i=-\infty}^{\infty} \sum_{j=-\infty}^{\infty} a_i^{(k)*} a_j^{(m)} \int_0^T h_c(t - iT_c) h_c(t + \tau - jT_c) \mathrm{d}t. \end{aligned} \tag{9.30}$$

The integral in (9.30) is non-zero only where the chip pulses $h_c(t - iT_c)$ and $h_c(t + \tau - jT_c)$ overlap. Since the delay τ can assume any value let $\tau = \ell T_c + \delta$, where $\ell = \lfloor \tau / T_c \rfloor$ is an integer and $0 \leq \delta < T_c$. If the chip pulses are chosen to have duration T_c and $\tau = \ell T_c + \delta$, then the chip pulses overlap only for $i = \ell + j$ and $i = \ell + j + 1$, so that

$$\begin{aligned} R_{k,m}(\tau) &= \frac{1}{2N} \sum_{i=0}^{N-1} a_i^{(k)*} a_{\ell+i}^{(m)} \frac{1}{T_c} \int_0^{T_c - \delta} h_c(t') h_c(t' + \delta) \mathrm{d}t' \\ &\quad + \frac{1}{2N} \sum_{i=0}^{N-1} a_i^{(k)*} a_{\ell+i+1}^{(m)} \frac{1}{T_c} \int_{T_c - \delta}^{T_c} h_c(t') h_c(t' - T_c + \delta) \mathrm{d}t'. \end{aligned} \tag{9.31}$$

The continuous-time partial autocorrelation functions of the chip waveform $h_c(t)$ (of duration T_c) are defined as [273]

$$R_h(\delta) = \frac{1}{T_c} \int_0^{T_c - \delta} h_c(t') h_c(t' + \delta) \mathrm{d}t' \tag{9.32}$$

$$\hat{R}_h(\delta) = \frac{1}{T_c} \int_{T_c - \delta}^{T_c} h_c(t') h_c(t' - T_c + \delta) \mathrm{d}t' \tag{9.33}$$

allowing us to write

$$R_{k,m}(\tau) = \phi_{k,m}(\ell) R_h(\delta) + \phi_{k,m}(\ell + 1) \hat{R}_h(\delta), \tag{9.34}$$

[3] For real-value spreading waveforms, the full period cross-correlation function is similar except for the factor of 1/2 in front of the integral.

where $\phi_{k,m}(\ell)$ is the full period cross-correlation defined in (9.20). For example, if $h_c(t) = u_{T_c}(t)$, then

$$R_{k,m}(\tau) = \phi_{k,m}(\ell)\left(1 - \frac{\delta}{T_c}\right) + \phi_{k,m}(\ell+1)\frac{\delta}{T_c}. \tag{9.35}$$

When $G < N$, the partial correlations in (9.22) and (9.23) must be used. In this case the cross-correlation in (9.34) becomes a random variable that (for random spreading sequences) has mean and variance

$$\mu_{R_{k,m}(\tau)} = \mu_{\phi_{k,m}(\ell)} R_h(\delta) + \mu_{\phi_{k,m}(\ell+1)} \hat{R}_h(\delta) = 0 \tag{9.36}$$

$$\sigma^2_{R_{k,m}(\tau)} = \sigma^2_{\phi_{k,m}(\ell)} R_h^2(\delta) + \sigma^2_{\phi_{k,m}(\ell+1)} \hat{R}_h^2(\delta) = \frac{1}{G}\left(R_h^2(\delta) + \hat{R}_h^2(\delta)\right). \tag{9.37}$$

Likewise, the autocorrelation is also a random variable that (for random spreading sequences) has mean and variance

$$\begin{aligned} \mu_{R_{k,k}(\tau)} &= \mu_{\phi_{k,k}(\ell)} R_h(\delta) + \mu_{\phi_{k,k}(\ell+1)} \hat{R}_h(\delta) \\ &= \begin{cases} R_h(\delta)\,, & \ell = iG \\ \hat{R}_h(\delta)\,, & \ell + 1 = iG \\ 0\,, & \text{elsewhere} \end{cases} \end{aligned} \tag{9.38}$$

$$\begin{aligned} \sigma^2_{R_{k,k}(\tau)} &= \sigma^2_{\phi_{k,k}(\ell)} R_h^2(\delta) + \sigma^2_{\phi_{k,k}(\ell+1)} \hat{R}_h^2(\delta) \\ &= \begin{cases} R_h^2(\delta)\,, & \ell = iG \\ \hat{R}_h^2(\delta)\,, & \ell + 1 = iG \\ 1/G\,, & \text{elsewhere} \end{cases} \end{aligned} \tag{9.39}$$

where i is an integer.

9.2.2 m-sequences

One very well-known and important class of spreading sequences are the maximal-length sequences or m-sequences. As shown in Fig. 9.6, an m-sequence $\tilde{\mathbf{a}} = \{\tilde{a}_k\}$, $\tilde{a}_k \in \{0, 1\}$, is generated by using a linear feedback shift register (LFSR) of length m. The sequence $\mathbf{a} = \{a_k\}$ is obtained by using the level shift $a_k = 2\tilde{a}_k - 1$. The feedback or connection polynomial in the LFSR is a primitive polynomial of degree m over GF(2), having the form

$$p(x) = 1 + p_1 x + p_2 x^2 + p_3 x^3 + \cdots + p_{m-1} x^{m-1} + x^m, \tag{9.40}$$

where $p_i \in \{0, 1\}$. Tables of primitive polynomials, $p(x)$, are tabulated in many texts, e.g., [203]. Notice that $p_0 = 1$, since this represents the feedback connection tap. Also, $p_m = 1$; otherwise, if $p_m = 0$, the effective length of the shift register is less than m.

Maximal length sequences are by definition the longest sequences that can be generated by an LFSR of a given length. For a shift register of length m, a sequence of length $N = 2^m - 1$ is generated. As an m-sequence generator cycles through

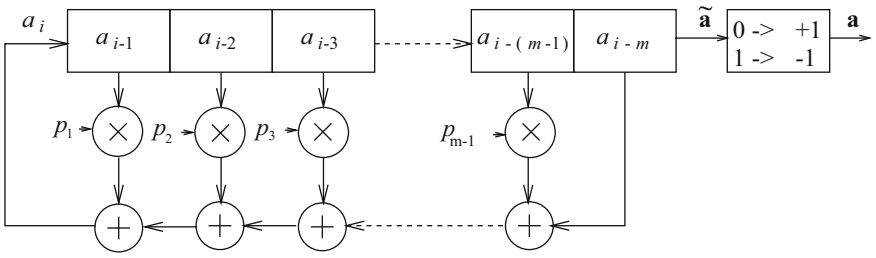

Fig. 9.6 m-sequence generator

one full period of length $N = 2^m - 1$, the contents of the m-stage shift register go through all possible $2^m - 1$ non-binary m-tuples values or states. The all-zeroes state is the only forbidden m-tuple, since the LFSR would lock in this state.

The m-sequences have many remarkable properties, and every full period of an m-sequence satisfies some important randomness properties. First, the sequence is nearly balanced with 2^{m-1} ones and $2^{m-1} - 1$ zeros. A run is defined as a string of consecutive zeros or ones, and a sequence can be characterized in terms of its run length distribution. For m-sequences the number of runs of length P, n_P, is

$$n_P = \begin{cases} 2^{m-P-1}, & P = 1, 2, \ldots, m-1 \\ 1, & P = m \end{cases}. \tag{9.41}$$

The full period autocorrelation of an m-sequence is

$$\phi(n) = \begin{cases} 1 & , \ n = \ell N \\ -1/N & , \ n \neq \ell N \end{cases}. \tag{9.42}$$

For large values of N, $\phi(n) \approx \delta(n)$ so that m-sequences are almost ideal in terms of their full period autocorrelation. For a rectangular chip shaping function $h_c(t) = u_{T_c}(t)$, the corresponding spreading waveform $a(t)$ has autocorrelation function

$$R(\tau) = \phi(\ell)\left(1 - \frac{\delta}{T_c}\right) + \phi(\ell + 1)\frac{\delta}{T_c}. \tag{9.43}$$

This function is plotted in Fig. 9.7.

The mean and variance of the partial period autocorrelation of an m-sequence can be obtained in a straightforward fashion by replacing the expectations in (9.25) and (9.27) with averages over all possible starting positions. This gives

$$\mu_{\phi(n)} = \begin{cases} 1 & , \ n = \ell N \\ -1/G & , \ n \neq \ell N \end{cases} \tag{9.44}$$

$$\sigma^2_{\phi(n)} = \begin{cases} 0 & , \ n = \ell N \\ \frac{1}{G}\left(1 + \frac{1}{N}\right)\left(1 - \frac{G}{N}\right) & , \ n \neq \ell N \end{cases}. \tag{9.45}$$

Unfortunately, m-sequences also have a number of undesirable properties. First, the number of m-sequences that can be generated by an LFSR of length m is equal to the number of primitive polynomials of degree m over GF(2), and is given by $\Phi(2^m - 1)/m$, where $\Phi(\cdot)$ is the Euler Totient function

$$\Phi(n) = n \prod_{p|n}^{n} \left(1 - \frac{1}{p}\right), \tag{9.46}$$

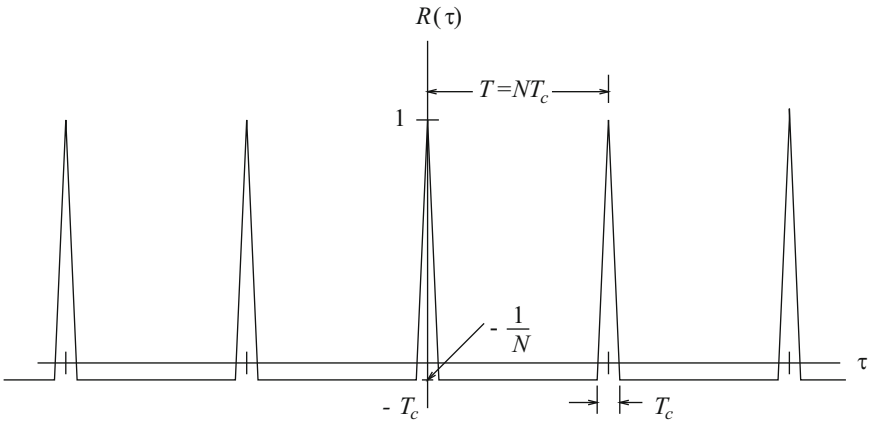

Fig. 9.7 Typical full period autocorrelation function of an m-sequence spreading waveform

Table 9.1 Best and worst case average cross-correlations for m-sequences

m	N	Number of m-sequences	θ worst	θ best
5	31	6	0.35	0.29
6	63	6	0.36	0.24
7	127	18	0.32	0.13
8	255	16	0.37	0.12
9	511	48	0.22	0.06
10	1023	60	0.37	0.06
11	2047	176	0.14	0.03
12	4095	144	0.34	0.03

where the product is over all primes p that divide n. Hence, there are relatively few m-sequences for a given shift register length m. Second, only for certain values of m, do there exist a few pairs of m-sequences with low full period cross-correlations. In general, m-sequences do not have good cross-correlation properties. Consider the full period cross-correlation $\phi_{k,m}(n)$ between two m-sequences $\mathbf{a}^{(k)}$ and $\mathbf{a}^{(m)}$. Let us define the average full period cross-correlation

$$\theta = \frac{1}{N}\sum_{n=0}^{N-1}\phi_{k,m}(n). \tag{9.47}$$

The value of θ depends on the particular pair of m-sequences that are selected. The best and worst case values of θ are shown in Table 9.1. Notice that the worst case full period cross-correlations are very large even for long sequence lengths.

9.2.3 Gold Sequences

A set of Gold sequences [141] consists of $2^m + 1$ sequences each with a period of $N = 2^m - 1$ that are generated by using a preferred pair of m-sequences obtained as follows. Let GF(2^m) be an extension field of GF(2). Let α be a primitive Nth root of unity in the extension field GF(2^m), where $N = 2^m - 1$. Let $p_1(x)$ and $p_2(x)$ be a pair of primitive polynomials over GF(2) each having degree m such that $p_1(\alpha) = 0$ and $p_2(\alpha^d) = 0$ for some integer d. Consider the case when $m \neq 0 \bmod 4$. If $d = 2^h + 1$ or $d = 2^{2h} - 2^h + 1$ and if $e = \text{GCD}(m, h)$ is such that m/e is odd, then $p_1(x)$ and $p_2(x)$ constitute a preferred pair of polynomials. Note that $p_2(x)$ may not be unique. For example, with $m = 5$, both $h = 1$ and $h = 2$ will work, so that either $p_2(x^3) = 0$ or $p_2(x^5) = 0$ may be chosen. To find the corresponding polynomials, the reader is referred to Peterson's table of irreducible polynomials [262]. The two m-sequences $\mathbf{a}^{(1)}$ and $\mathbf{a}^{(2)}$ that are generated by using $p_1(x)$ and $p_2(x)$ are known as a preferred pair of m-sequences. Their cross-correlation function is three-valued with the values $\{-1, -t(m), t(m) - 2\}$, where

$$t(m) = \begin{cases} 2^{(m+1)/2} + 1 & , \ m \text{ odd} \\ 2^{(m+2)/2} + 1 & , \ m \text{ even} \end{cases}. \tag{9.48}$$

By using the preferred pair of sequences $\mathbf{a}^{(1)}$ and $\mathbf{a}^{(2)}$, a set of Gold sequences can be constructed by taking the sum of $\mathbf{a}^{(1)}$ with all cyclically shifted versions of $\mathbf{a}^{(2)}$ or vice versa. A typical Gold sequence generator is shown in Fig. 9.8, where the preferred pair of polynomials are $p_1(x) = 1 + x^2 + x^5$ and $p_2(x) = 1 + x + x^2 + x^4 + x^5$. This above procedure yields N new sequences each with period $N = 2^m - 1$. These sequences along with the original two sequences give a set of $2^m + 1$ Gold sequences.

It is important to note that not all the $2^m + 1$ Gold sequences are balanced with 2^{m-1} ones and $2^{m-1} - 1$ zeros. In fact, it can be shown that only $2^m - 2^{m-e} - 1$ of the Gold sequences are so balanced. The balanced Gold sequences are the most desirable. With the exception of the preferred pair of sequences $\mathbf{a}^{(1)}$ and $\mathbf{a}^{(2)}$, the Gold sequences are not m-sequences and, therefore, their autocorrelation functions are not two-valued. However, Gold sequences have three-valued off-peak autocorrelations and cross-correlations, with possible values $\{-1, -t(m), t(m) - 2\}$, where $t(m)$ is defined in (9.48). The cross-correlation properties of m-sequences and Gold sequences are summarized in Table 9.2. Notice that Gold sequences have much smaller peak cross-correlations than m sequences.

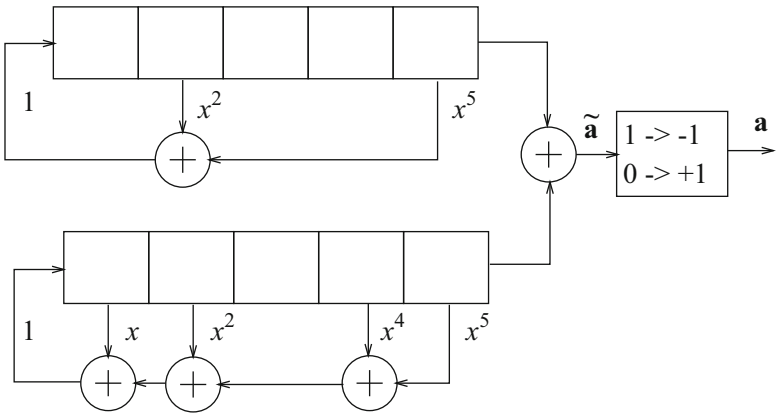

Fig. 9.8 A Gold sequence generator with $p_1(x) = 1 + x^2 + x^5$ and $p_2(x) = 1 + x + x^2 + x^4 + x^5$. This sequence generator can produce 32 Gold sequences of length 31

Table 9.2 Peak cross-correlation of *m*-sequences and Gold sequences

m	N	Number m sequences	Peak cross-correlation	m-sequence $\phi_{\max}/\phi(0)$	$t(m)$	Gold sequence $t(m)/\phi(0)$
3	7	2	5	0.71	5	0.71
4	15	2	9	0.60	9	0.60
5	31	6	11	0.35	9	0.29
6	63	6	23	0.36	17	0.27
7	127	18	41	0.32	17	0.13
8	255	16	95	0.37	33	0.13
9	511	48	113	0.22	33	0.06
10	1023	60	383	0.37	65	0.06
11	2047	176	287	0.14	65	0.03
12	4095	144	1407	0.34	129	0.03

9.2.4 Kasami Sequences

The construction of Kasami sequences proceeds as follows [175, 176]. Let m be even. Let $p_1(x)$ be a primitive polynomial over the binary field GF(2) with degree m and α as a root, and let $p_2(x)$ be the irreducible minimal polynomial of α^d where $d = 2^{m/2} + 1$. Once again, these polynomials can be identified using Peterson's table of irreducible polynomials [262]. Let $\mathbf{a}^{(1)}$ and $\mathbf{a}^{(2)}$ represent the two m-sequences of periods $2^m - 1$ and $2^{m/2} - 1$ that are generated by $p_1(x)$ and $p_2(x)$, respectively. The set of Kasami sequences is generated by using the two m-sequences in a fashion similar to the generation of Gold sequences, i.e., the set of Kasami sequences consists of the long sequence $\mathbf{a}^{(1)}$ and the sum of $\mathbf{a}^{(1)}$ with all $2^{m/2} - 1$ cyclic shifts of the short sequence $\mathbf{a}^{(2)}$. The number of Kasami sequences in the set is $2^{m/2}$, each having period $N = 2^m - 1$. In fact, this set is known as the *small set* of Kasami sequences. A typical Kasami sequence generator is shown in Fig. 9.9 with generator polynomials $p_1(x) = 1+x+x^6$ and $p_2(x) = 1+x+x^3$. Like Gold sequences, the off-peak autocorrelation and cross-correlation functions of Kasami sequences are also three-valued, however, the possible values are $\{-1, -s(m), s(m) - 2\}$, where $s(m) = 2^{m/2} + 1$.

9.2.5 Barker Sequences

Barker sequences only exist for lengths 2, 3, 4, 5, 7, 11, and 13, given as follows:

$$\mathbf{a} = (+1 - 1)$$

$$\mathbf{a} = (+1 + 1 - 1)$$

$$\mathbf{a} = (+1 + 1 - 1 + 1)$$

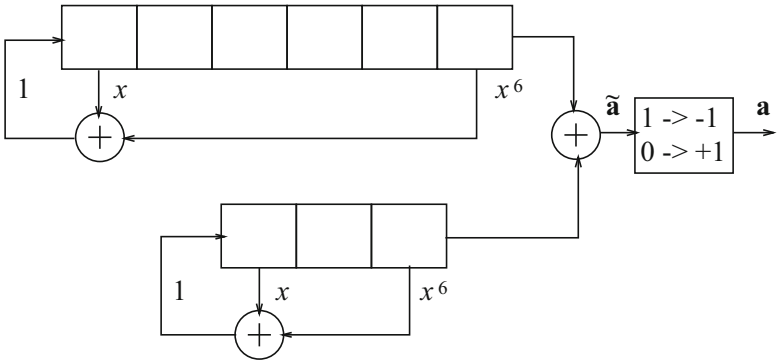

Fig. 9.9 A Kasami sequence generator with $p_1(x) = 1+x+x^6$ and $p_2(x) = 1+x+x^3$. This sequence generator can produce 8 Kasami sequences of length 63

$$\mathbf{a} = (+1+1+1-1+1)$$
$$\mathbf{a} = (+1+1+1-1-1+1-1)$$
$$\mathbf{a} = (+1+1+1-1-1-1+1-1-1+1-1)$$
$$\mathbf{a} = (+1+1+1+1+1-1-1+1+1-1+1-1+1)$$

The mirror images (or time reversed) sequences are also Barker sequences. Barker sequences of other lengths do not exist. Barker sequences are specially designed sequences that have almost ideal aperiodic autocorrelation functions, as defined in (9.21). For the Barker sequences

$$\phi^a_{k,k}(n) = \begin{cases} 1 & , \quad n = 0 \\ 0, 1/N, \text{or} -1/N & , \quad 1 \leq |n| \leq N-1 \end{cases} . \tag{9.49}$$

9.2.6 Walsh-Hadamard Sequences

Walsh-Hadamard sequences are obtained by selecting as sequences the rows of a Hadamard matrix $\mathbf{H}_M$. For $M = 2$ the Hadamard matrix is

$$\mathbf{H}_2 = \begin{bmatrix} +1 & +1 \\ +1 & -1 \end{bmatrix}. \tag{9.50}$$

Larger Hadamard matrices are obtained by using the recursion

$$\mathbf{H}_{2M} = \begin{bmatrix} \mathbf{H}_M & \mathbf{H}_M \\ \mathbf{H}_M & -\mathbf{H}_M \end{bmatrix}. \tag{9.51}$$

For example,

$$\mathbf{H}_8 = \begin{bmatrix} +1 & +1 & +1 & +1 & +1 & +1 & +1 & +1 \\ +1 & -1 & +1 & -1 & +1 & -1 & +1 & -1 \\ +1 & +1 & -1 & -1 & +1 & +1 & -1 & -1 \\ +1 & -1 & -1 & +1 & +1 & -1 & -1 & +1 \\ +1 & +1 & +1 & +1 & -1 & -1 & -1 & -1 \\ +1 & -1 & +1 & -1 & -1 & +1 & -1 & +1 \\ +1 & +1 & -1 & -1 & -1 & -1 & +1 & +1 \\ +1 & -1 & -1 & +1 & -1 & +1 & +1 & -1 \end{bmatrix}. \tag{9.52}$$

The rows in the Hadamard matrix define the Walsh-Hadamard sequences, and have the property that they are mutually orthogonal.

The Walsh-Hadamard sequences can be used for orthogonal spreading, also called orthogonal CDMA, where the users are distinguished by assigning them different Walsh-Hadamard sequences, and the data symbols are sent by using simple binary spreading as shown in Fig. 9.4. With orthogonal CDMA, the data symbols of the different users must be synchronized to within a small fraction of a chip period. This is because the Walsh-Hadamard sequences have very poor cross-correlations at non-zero lags. In fact, some of the Walsh-Hadamard sequences are just cyclic shifts of each other. Finally, multipath will also destroy the orthogonality of the received waveforms, because the Walsh Hadamard sequences have large off-peak autocorrelation values even at small lags. This will lead to multiple-access interference in orthogonal CDMA systems.

9.2.6.1 Orthogonal and Bi-orthogonal Modulation

The Walsh Hadamard sequences can be used for modulation rather than spreading. There are several possibilities. One is M-ary orthogonal modulation, where $k = \log_2 M$ bits are used to select one of the M orthogonal waveforms for transmission. The signals can be detected coherently or non-coherently as discussed in Chap. 5. Another possibility is a variant of biorthogonal modulation, where each row of the Hadamard matrix is used to send one bit of information. In this case M bits are sent at one time. This type of modulation requires coherent detection.

9.2.7 Variable Length Orthogonal Codes

For multimedia applications, it is necessary to support a variety of data streams ranging from low to very high bit rates. Quite often these streams are used concurrently and they all use the same spread bandwidth. Consider a system where each data symbol in the highest bit rate stream $R = R_{\max}$ is spread by an orthogonal sequence of length $N = 2^m$. Then the data symbols in a stream with bit rate $R = R_{\max}/2^k$ are spread by a sequence of length 2^{m+k}. One way to achieve orthogonality between spreading sequences with different spreading factors is to use tree-structured orthogonal codes. The construction of these codes is illustrated in Fig. 9.10. Tree-structured orthogonal codes are generated recursively according to the following:

$$\mathbf{c}_{2n} = \begin{bmatrix} \mathbf{c}_{2n,1} \\ \mathbf{c}_{2n,2} \\ \vdots \\ \mathbf{c}_{2n,2n} \end{bmatrix} = \begin{bmatrix} \begin{bmatrix} \mathbf{c}_{n,1} & \mathbf{c}_{n,1} \\ \mathbf{c}_{n,1} & -\mathbf{c}_{n,1} \end{bmatrix} \\ \vdots \\ \begin{bmatrix} \mathbf{c}_{n,n} & \mathbf{c}_{n,n} \\ \mathbf{c}_{n,n} & -\mathbf{c}_{n,n} \end{bmatrix} \end{bmatrix} \tag{9.53}$$

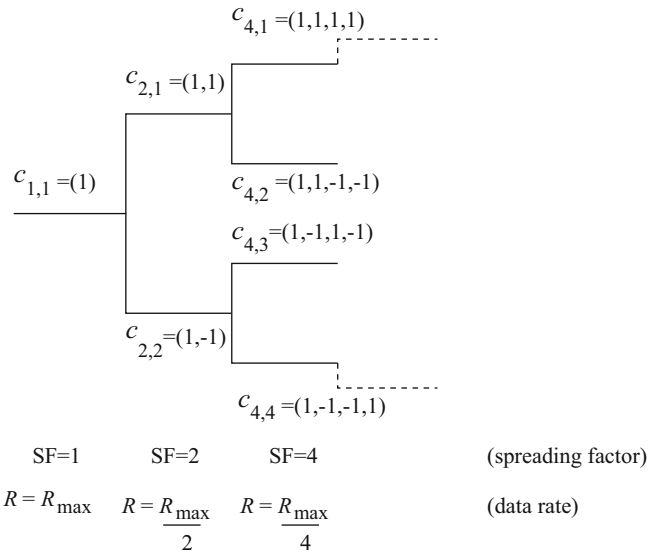

Fig. 9.10 Construction of orthogonal spreading codes with different spreading factors

where $\mathbf{c}_{2n}$ is an orthogonal code set of size $2n$. The orthogonality properties are similar to Walsh-Hadamard sequences. In fact the set of sequences is identical, and only their order is different.

A code can be assigned for use if and only if no other code either on the path from the specific code to the root of the tree, or on the subtree produced by the specific code, is already being used. Hence, the total number of available codes is not fixed, but depends on the rate or spreading factor of each physical channel.

9.2.8 Complementary Code Keying

Complementary codes have the property that the sum of their aperiodic autocorrelation functions is zero for all delays except zero delay. That is,

$$\frac{1}{M}\sum_{k=1}^{M}\phi_{k,k}^{a}(n) = \delta(n). \tag{9.54}$$

A variety of constructions exist for complementary codes and two examples are given here. The IEEE 802.11b standard uses length-8 CCK sequences for 11 Mb/s transmission. The eight complex chip values for CCK code words are

$$\begin{aligned}\mathscr{C} = \big\{&e^{j(\phi_1+\phi_2+\phi_3+\phi_4)}, e^{j(\phi_1+\phi_3+\phi_4)}, e^{j(\phi_1+\phi_2+\phi_4)},\\ &-e^{j(\phi_1+\phi_4)}, e^{j(\phi_1+\phi_2+\phi_3)}, e^{j(\phi_1+\phi_3)}, -e^{j(\phi_1+\phi_2)}, e^{j(\phi_1)}\big\},\end{aligned} \tag{9.55}$$

where the phases $\{\phi_1, \phi_2, \phi_3, \phi_4\}$ are QPSK phases. The phases ϕ_2, ϕ_3, and ϕ_4 each take on four different values, leading to a code alphabet of size 64. The phase ϕ_1 is differentially encoded across successive codewords. Since each of the four phases ϕ_1 to ϕ_4 represents 2 bits of information, 8 bits are transmitted per codeword. The chip rate for IEEE 802.11 is 11 Mchips/s, so that the resulting bit rate is 11 Mb/s.

The IEEE 802.11b standard for 5.5 Mb/s transmission is similar but uses CCK with length-4 sequences. The complex chip values for the CCK code words are

$$\mathscr{C} = \big\{e^{j(\phi_1+\phi_2+\phi_3)}, e^{j(\phi_1+\phi_3)}, e^{j(\phi_1+\phi_2)}, -e^{j(\phi_1)}\big\}, \tag{9.56}$$

where, again, the phases $\{\phi_1, \phi_2, \phi_3\}$ are QPSK phases.

9.2.9 Zadoff–Chu Sequences

A Zadoff–Chu sequence, sometimes called a Chu sequence [64], is a complex-valued sequence defined in the time domain by the following:

$$a_n^{(m)} = \begin{cases} e^{-j\frac{\pi m n^2}{N}}, & \text{when } N \text{ is even} \\ e^{-j\frac{\pi m n(n+1)}{N}}, & \text{when } N \text{ is odd} \end{cases} \qquad 0 \le n \le N-1 \tag{9.57}$$

where m is called the sequence index or family, such that m is relatively prime to the sequence length N (meaning that the only integer that divides m and N is 1). The number of Zadoff–Chu sequences for a given length N is the number of integers that are relatively prime to N. Thus, to maximize the number of available Zadoff–Chu sequences for a given sequence length N, N may be chosen to be a prime number.

The DFT of the Zadoff–Chu sequence in (9.57) for N even can be obtained from the table of DFT pairs in [75] as

$$A_k^{(m)} = e^{j\pi\left(\frac{(N-k)^2}{mN}-\frac{1}{4}\right)}\frac{1}{\sqrt{m}}\sum_{\ell=0}^{m-1}\xi^{\ell(n-k)-\ell^2 N/2} \tag{9.58}$$

where $m > 0$, mN is even, and $\xi = \mathrm{e}^{-j2\pi/m}$. When $m = 1$ this reduces to

$$A_k^{(1)} = \mathrm{e}^{-j\pi/4}\mathrm{e}^{j\pi k^2}. \tag{9.59}$$

An important property of Zadoff–Chu sequences is their orthogonality to their cyclic shifts. Lemma 9.1 below provides a general theorem for circular *auto-orthogonality*.

Lemma 9.1. *If and only if a sequence* $\{A_k\}$, $k = 0, \cdots, N-1$, *is circular auto-orthogonal, i.e.,*

$$\frac{1}{N}\sum_{k=0}^{N-1} A_k A^*_{(k-l)_N} = \delta_l = \begin{cases} 1 \ , & l = 0 \\ 0 \ , & l \neq 0 \end{cases}, \tag{9.60}$$

meaning that A_k *is orthogonal to any of its cyclic shifts, then the time domain sequence* $\{a_k\}$, $k = 0, \cdots, N-1$, *has constant envelope.*

Proof. The proof can be carried out by manipulating properties of the DFT. Since $|a_n|^2 = a_n a_n^*$, $a_n \overset{\text{DFT}}{\longrightarrow} A_k$, and $a_n^* \overset{\text{DFT}}{\longrightarrow} A^*_{(-k)_N}$,

$$|a_n|^2 = a_n a_n^* \overset{\text{DFT}}{\longrightarrow} A_k \circledast A^*_{(-k)_N} = \frac{1}{\sqrt{N}}\sum_{l=0}^{N-1} A_l A^*_{(l-k)_N}, \tag{9.61}$$

where $\circledast$ is circular convolution. If $\{A_k\}$ is circular auto-orthogonal, then the right side of (9.61) is equal to $\sqrt{N}\delta_k$. This leads to $a_n a_n^* = 1$ and, therefore, $|a_n| = 1$. Conversely, if $|a_n| = 1$, then $a_n a_n^* = 1$, and its DFT is $\sqrt{N}\delta_k$. From (9.61), $A_k \circledast A^*_{(-k)_N} = \sqrt{N}\delta_k$. Therefore, $\{A_k\}$ is circular auto-orthogonal. From the fact $a_n \overset{\text{DFT}}{\longrightarrow} A_k$ and $|a_n| = |A_k| = 1$ both sequences a_n and A_k are circular auto-orthogonal, based on Lemma 9.1.

Zadoff–Chu sequences have the following useful properties:

- Constant Envelope: The Zadoff–Chu sequences have constant envelope in the time domain.
- Auto-orthogonal: The Zadoff–Chu sequences have a perfect periodic autocorrelation in the time domain

$$\phi_{m,m}(n) = \frac{1}{N_{\text{ZC}}}\sum_{i=0}^{N_{\text{ZC}}-1} a_i^{(m)^*} a_{i+n}^{(m)} = \delta(n) \ , \quad n = 0, \ldots, N_{\text{ZC}} - 1. \tag{9.62}$$

- Low Cross-correlations: The cross-correlation of two different prime length Zadoff–Chu sequences of family m_1 and m_2 is a constant $1/\sqrt{N_{\text{ZC}}}$ regardless of time shift, provided that $m_1 - m_2$ is relatively prime to N_{ZC}.

Example 9.1. Consider the special DFT pair [75]

$$\begin{aligned} a_n &= \mathrm{e}^{-j\frac{\pi}{8}}\mathrm{e}^{j\frac{\pi n^2}{N}}, \quad n = 0, \cdots, N-1 \\ A_k &= \mathrm{e}^{j\frac{\pi}{8}}\mathrm{e}^{-j\frac{\pi k^2}{N}}, \quad k = 0, \cdots, N-1, \end{aligned} \tag{9.63}$$

This particular DFT pair satisfies all the properties of Zadoff–Chu sequences and, moreover, $A_k = a_k^*$ so the DFT sequence of the a_n is simply its conjugate. In the time domain, the sequence a_n serves as a perfect synchronization sequence, having unity peak-to-average power ratio (PAPR). Meanwhile, the sequence A_k has constant envelope in the frequency domain. This property simplifies the process of channel estimation in the frequency domain since the sub-carriers are excited with known training symbols of equal power, such that the power spectrum of the pilot waveform is flat over the bandwidth of interest.

9.3 Power Spectral Density of DS Spread Spectrum Signals

The DS/QPSK waveform can be thought of as a QPSK waveform where the nth data symbol is transmitted with the amplitude shaping pulse in (9.5). For uncorrelated zero-mean data symbols, the results in Sect. 4.9.1.2 show that the power spectral density (psd) of the DS/QPSK complex envelope is c.f. (4.218)

$$S_{\widetilde{s}\widetilde{s}}(f) = \frac{A^2}{T}\sigma_x^2 \left|H_a(f)\right|^2, \tag{9.64}$$

where $h_a(t)$ is the amplitude shaping pulse. In the case of a short code, the amplitude shaping pulse is

$$h_a(t) = \sum_{k=0}^{N-1} a_k h_c(t - kT_c). \tag{9.65}$$

Taking the Fourier transform of $h_a(t)$ gives

$$H_a(f) = H_c(f) \sum_{k=0}^{N-1} a_k \mathrm{e}^{-j2\pi fkT_c} \tag{9.66}$$

and

$$\left|H_a(f)\right|^2 = \left|H_c(f)\right|^2 \sum_{k=0}^{N-1}\sum_{\ell=0}^{N-1} a_k a_\ell^* \mathrm{e}^{-j2\pi f(k-\ell)T_c}. \tag{9.67}$$

The above expression can be put in a more convenient form by using the aperiodic autocorrelation defined in (9.21). It can be shown that

$$\left|H_a(f)\right|^2 = \left|H_c(f)\right|^2 2N\Phi^a(f), \tag{9.68}$$

where $\Phi^a(f)$ is the discrete-time Fourier transform (DTFT) of the aperiodic autocorrelation function, defined by

$$\Phi^a(f) = \sum_{n=-N+1}^{N-1} \phi^a(n)\mathrm{e}^{-j2\pi fnT_c}. \tag{9.69}$$

Using $T = NT_c$ and $\sigma_x^2 = \frac{1}{2}\mathrm{E}[|x_i|^2] = 1/2$ gives

$$S_{\widetilde{s}\widetilde{s}}(f) = \frac{A^2}{T_c}\left|H_c(f)\right|^2 \Phi^a(f). \tag{9.70}$$

Observe that the psd depends on both $|H_c(f)|$ and $\Phi^a(f)$. Suppose the spreading sequence has an ideal "thumbtack" aperiodic autocorrelation function

$$\phi^a(n) = \begin{cases} 1\,, & n = 0 \\ 0\,, & n \neq 0 \end{cases}. \tag{9.71}$$

Then $\Phi^a(f) = 1$ and

$$S_{\widetilde{s}\widetilde{s}}(f) = \frac{A^2}{T_c}\left|H_c(f)\right|^2. \tag{9.72}$$

In this case, the psd depends only on the chip shaping response $|H_c(f)|$. For example, if $h_c(t) = u_{T_c}(t)$, then $H_c(f) = T_c\mathrm{sinc}(fT_c)$ and $S_{\widetilde{s}\widetilde{s}}(f) = A^2T_c\mathrm{sinc}^2(fT_c)$. Unfortunately, spreading sequences having the ideal aperiodic autocorrelation function in (9.71) do not exist for any non-trivial length. Consider the two sequences:

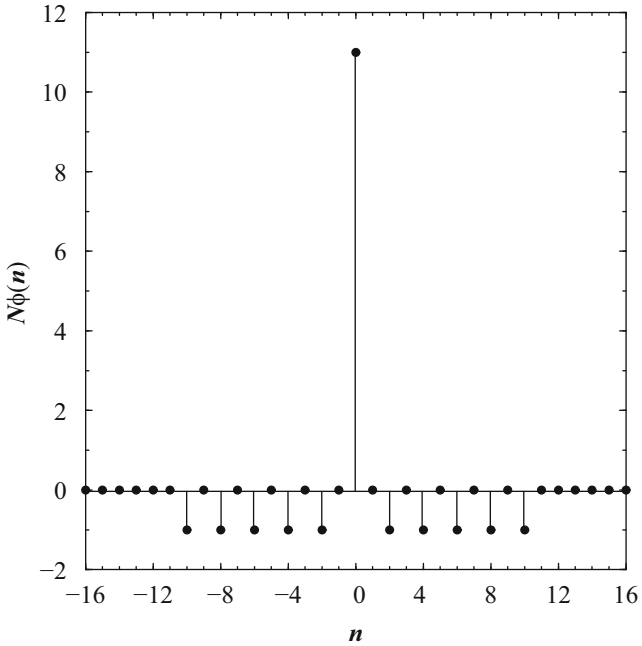

Fig. 9.11 Aperiodic autocorrelation function for the length-11 Barker sequence

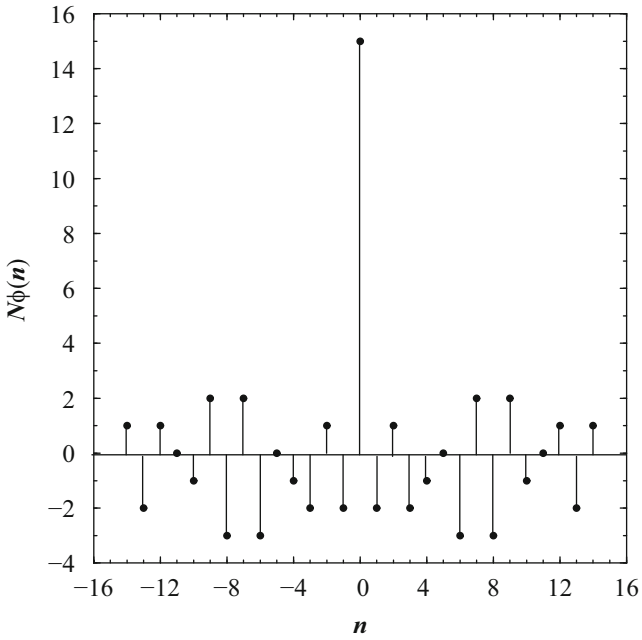

Fig. 9.12 Aperiodic autocorrelation function for the length-15 *m*-sequence

$$\mathbf{a}^{(1)} = (-1+1-1-1+1-1-1-1+1+1+1) \tag{9.73}$$
$$\mathbf{a}^{(2)} = (+1-1-1+1-1-1-1+1+1+1+1-1+1-1+1).$$

The first is a length-11 Barker sequence and the second is a length-15 *m*-sequence. The scaled aperiodic autocorrelation functions $N\phi^a(n)$ for these sequences are shown in Figs. 9.11 and 9.12, respectively.

The corresponding power spectral densities with the rectangular chip shaping function $h_c(t) = u_{T_c}(t)$ are plotted in Figs. 9.13 and 9.14, respectively. Notice that the aperiodic autocorrelation of the *m*-sequence deviates significantly from the ideal function in (9.71). This leads to peaks and nulls in the spectrum shown in Fig. 9.14. Such spectral peaks are undesirable.

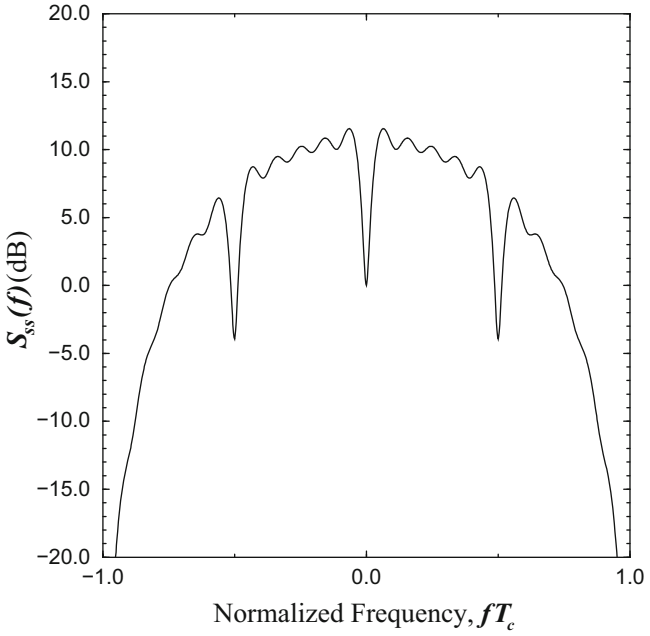

Fig. 9.13 Psd with the length-11 Barker sequence

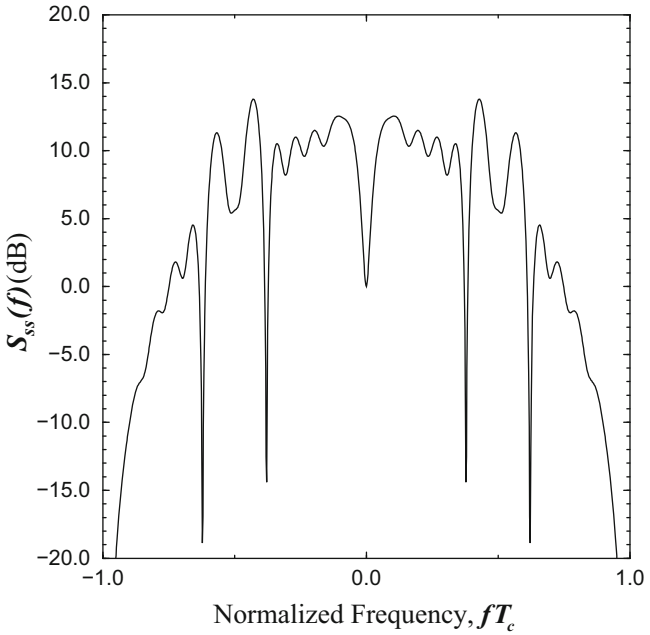

Fig. 9.14 Psd with the length-15 *m*-sequence

The length-11 Barker sequence is seen to provide a much smoother psd without any large peaks. For this reason, and the fact that a minimum length-10 sequence is required by the IEEE 802.11 WLAN standard, the length-11 Barker sequence was chosen.

It is interesting to note that if CCK is used, then the psd depends on the DTFT of the average aperiodic autocorrelation function in (9.54). In this case,

$$\frac{1}{M}\sum_{k=1}^{M}\Phi_{k,k}^{a}(f) = 1, \tag{9.74}$$

and the psd has the ideal form in (9.72). Finally, if a long code is used, then the power spectrum must be obtained by averaging over all possible spreading code subsequences of length G. Usually, this will result in a "smoother" power density spectrum.

9.4 Performance of DS/QPSK in CW Tone Interference

Spread spectrum systems must often operate in the presence of narrowband interference. This section examines the effect of continuous wave (CW) tone interference on the performance of DS/QPSK. Consider a DS/QPSK system with dual-channel quaternary spreading as shown in Fig. 9.3. The bandpass DS/QPSK waveform is

$$s(t) = A\sum_{n}\Big(x_{I,n}h_{I,n}(t-nT)\cos(2\pi f_c t) - x_{Q,n}h_{Q,n}(t-nT)\sin(2\pi f_c t)\Big), \tag{9.75}$$

where A is the amplitude. During time interval $[nT,(n+1)T)$ the transmitted quaternary data symbol is $x_n = (x_{I,n}, x_{Q,n})$, $x_{I,n}, x_{Q,n} \in \{+1/\sqrt{2}, -1/\sqrt{2}\}$ and the spreading waveforms are

$$h_{I,n}(t) = \sum_{k=0}^{G-1} a_{I,nG+k}h_c(t-nT_c)\ , \qquad h_{Q,n}(t) = \sum_{k=0}^{G-1} a_{Q,nG+k}h_c(t-nT_c). \tag{9.76}$$

With dual-channel quaternary spreading, the energy per modulated symbol is

$$\begin{aligned}
E &= \int_0^T s^2(t)\mathrm{d}t \\
&= A^2\int_0^T \left(x_{I,n}^2 h_{I,n}^2(t)\cos^2(2\pi f_c t) + x_{Q,n}^2 h_{Q,n}^2(t)\sin^2(2\pi f_c t)\right) \\
&= \frac{A^2}{4}\int_0^T \left(h_{I,n}^2(t) + h_{Q,n}^2(t)\right) \\
&= \frac{A^2}{4}\sum_{k=0}^{G-1}\left(a_{I,nG+k}^2 + a_{Q,nG+k}^2\right)\int_0^{T_c} h_c^2(t)\mathrm{d}t \\
&= G\frac{A^2}{2}\int_0^{T_c} h_c^2(t)\mathrm{d}t \\
&= GE_c,
\end{aligned} \tag{9.77}$$

where

$$E_c = \frac{A^2}{2}\int_0^{T_c} h_c^2(t)\mathrm{d}t \tag{9.78}$$

is the energy per PN chip. Note that (9.78) and (9.2) differ by a factor of 2, because (9.2) assumes complex spreading while (9.78) assumes quadrature spreading. This can be seen by comparing the energy of the bandpass waveforms in (9.6) and (9.75) over the interval $[nT,(n+1)T)$.

The received bandpass signal in the presence of continuous wave (CW) tone interference and additive white Gaussian noise (AWGN) is

$$r(t) = s(t) + n(t) + J(t), \tag{9.79}$$

where $n(t)$ is AWGN with two-sided power spectral density $N_o/2$ and $J(t)$ is the CW tone interference of the form

$$J(t) = A_J\cos(2\pi f_J t + \theta), \tag{9.80}$$

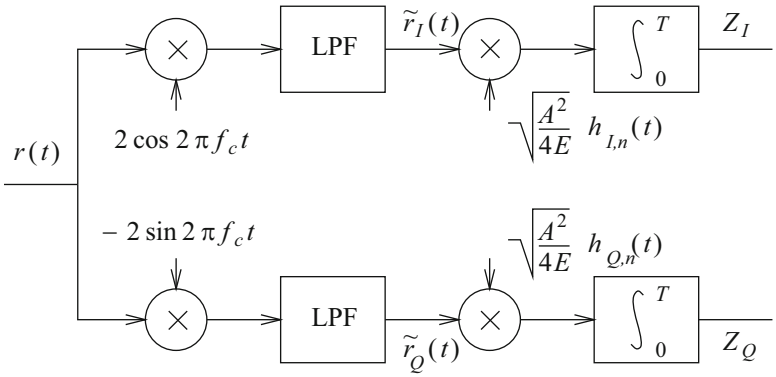

Fig. 9.15 Quadrature demodulator for DS/QPSK

where A_J is the tone amplitude, f_J is its frequency, and θ is a random phase uniformly distribution on the interval $[-\pi, \pi)$. The tone energy in a time interval of duration T is

$$E_J = \frac{A_J^2 T}{2}. \tag{9.81}$$

The received signal is despread and processed with the quadrature demodulator shown in Fig. 9.15 to generate the decision variables Z_I and Z_Q. To derive the values of Z_I and Z_Q the signal, noise, and interference terms are considered separately. During the time interval $[nT, (n+1)T)$ the contribution of the signal term to Z_I and Z_Q is

$$\begin{aligned} Z_I(s) &= \int_0^T \tilde{s}_I(t)\sqrt{\frac{A^2}{4E}}h_{I,n}(t)\mathrm{d}t \\ &= \int_0^T Ax_{I,n}h_{I,n}(t)\sqrt{\frac{A^2}{4E}}h_{I,n}(t)\mathrm{d}t \\ &= x_{I,n}A\sqrt{\frac{A^2}{4E}}\int_0^T h_{I,n}^2(t)\mathrm{d}t \\ &= x_{I,n}\sqrt{E}, \end{aligned} \tag{9.82}$$

where (9.77) was used. Likewise,

$$Z_Q(s) = x_{Q,n}\sqrt{E}. \tag{9.83}$$

The contribution of the AWGN term to Z_I and Z_Q is

$$Z_I(n) = \int_0^T \tilde{n}_I(t)\sqrt{\frac{A^2}{4E}}h_{I,n}(t)\mathrm{d}t \tag{9.84}$$

$$Z_Q(n) = \int_0^T \tilde{n}_Q(t)\sqrt{\frac{A^2}{4E}}h_{Q,n}(t)\mathrm{d}t. \tag{9.85}$$

It can be shown that $Z_I(n)$ and $Z_Q(n)$ are independent zero-mean Gaussian random variables with variance $N_o/2$.

Finally, the contribution of the CW tone interference term to Z_I and Z_Q can be calculated as follows:

$$\begin{aligned} Z_I(J) &= \int_0^T J(t)2\cos(2\pi f_c t)\sqrt{\frac{A^2}{4E}}h_{I,n}(t)\mathrm{d}t \\ &= \int_0^T A_J\cos(2\pi f_J t)2\cos(2\pi f_c t)\sqrt{\frac{A^2}{4E}}h_{I,n}(t)\mathrm{d}t \end{aligned}$$

$$
\begin{aligned}
&= A_J \sqrt{\frac{A^2}{4E}} \int_0^T 2h_{I,n}(t)\cos(2\pi f_c t)\cos(2\pi f_J t + \theta)\mathrm{d}t \\
&= A_J \sqrt{\frac{A^2}{4E}} \int_0^T h_{I,n}(t)\left\{\cos(2\pi \Sigma_f t + \theta) + \cos(2\pi \Delta_f t + \theta)\right\}\mathrm{d}t,
\end{aligned}
\tag{9.86}
$$

where

$$\Sigma_f = f_c + f_J \tag{9.87}$$

$$\Delta_f = f_J - f_c. \tag{9.88}$$

Using $A_J = \sqrt{2E_J/T}$ gives

$$Z_I(J) = \sqrt{E_J}\sqrt{\frac{A^2 T}{2E}}\frac{1}{T}\int_0^T h_{I,n}(t)\Big(\cos(2\pi \Sigma_f t + \theta) + \cos(2\pi \Delta_f t + \theta)\Big)\mathrm{d}t \tag{9.89}$$

Finally, using

$$E = G\frac{A^2}{2}\int_0^{T_c} h_c^2(t)\mathrm{d}t \tag{9.90}$$

gives

$$Z_I(J) = \sqrt{E_J/\bar{h_c}}\frac{1}{T}\int_0^T h_{I,n}(t)\Big(\cos(2\pi \Sigma_f t + \theta) + \cos(2\pi \Delta_f t + \theta)\Big)\mathrm{d}t, \tag{9.91}$$

where

$$\bar{h_c} = \frac{1}{T_c}\int_0^{T_c} h_c(t)\mathrm{d}t. \tag{9.92}$$

Using further trigonometric identities gives

$$
\begin{aligned}
Z_I(J) = \sqrt{E_J/\bar{h_c}}\Bigg(&\cos(\theta)\frac{1}{T}\int_0^T h_{I,n}(t)\Big(\cos(2\pi \Sigma_f t) + \cos(2\pi \Delta_f t)\Big)\mathrm{d}t \\
&- \sin(\theta)\frac{1}{T}\int_0^T h_{I,n}(t)\Big(\sin(2\pi \Sigma_f t) + \sin(2\pi \Delta_f t)\Big)\mathrm{d}t\Bigg).
\end{aligned}
\tag{9.93}
$$

In a similar fashion

$$
\begin{aligned}
Z_I(J) &= \int_0^T J(t)2\sin(2\pi f_c t)\sqrt{\frac{A^2}{4E}}h_{Q,n}(t)\mathrm{d}t \\
&= \sqrt{E_J/\bar{h_c}}\Bigg(\cos(\theta)\frac{1}{T}\int_0^T h_{Q,n}(t)\Big(\sin(2\pi \Delta_f t) - \sin(2\pi \Sigma_f t)\Big)\mathrm{d}t \\
&\quad + \sin(\theta)\frac{1}{T}\int_0^T h_{Q,n}(t)\Big(\cos(2\pi \Delta_f t) - \sin(2\pi \Sigma_f t)\Big)\mathrm{d}t\Bigg).
\end{aligned}
\tag{9.94}
$$

Combining the signal, noise, and CW tone interference terms gives

$$
\begin{aligned}
Z_I &= Z_I(s) + Z_I(n) + Z_I(J) \\
Z_Q &= Z_Q(s) + Z_Q(n) + Z_Q(J).
\end{aligned}
\tag{9.95}
$$

Hence, Z_I and Z_Q are independent Gaussian random variables with means

$$\begin{aligned} \mathrm{E}[Z_I] &= x_{I,n}\sqrt{E} + I_I\sqrt{E_J/\bar{h_c}} \\ \mathrm{E}[Z_Q] &= x_{Q,n}\sqrt{E} + I_Q\sqrt{E_J/\bar{h_c}}, \end{aligned} \tag{9.96}$$

and variance $N_o/2$, where

$$\begin{aligned} I_I &= \cos(\theta)\frac{1}{T}\int_0^T h_{I,n}(t)\Big(\cos(2\pi\Sigma_f t) + \cos(2\pi\Delta_f t)\Big)\mathrm{d}t \\ &\quad - \sin(\theta)\frac{1}{T}\int_0^T h_{I,n}(t)\Big(\sin(2\pi\Sigma_f t) + \sin(2\pi\Delta_f t)\Big)\mathrm{d}t \end{aligned} \tag{9.97}$$

$$\begin{aligned} I_Q &= \cos(\theta)\frac{1}{T}\int_0^T h_{Q,n}(t)\Big(\sin(2\pi\Delta_f t) - \sin(2\pi\Sigma_f t)\Big)\mathrm{d}t \\ &\quad + \sin(\theta)\frac{1}{T}\int_0^T h_{Q,n}(t)\Big(\cos(2\pi\Delta_f t) - \sin(2\pi\Sigma_f t)\Big)\mathrm{d}t. \end{aligned} \tag{9.98}$$

9.4.1 Short Code

For the purpose of illustration assume a rectangular chip shaping pulse $h_c(t) = u_{T_c}(t)$ so that $\bar{h_c} = 1$ in (9.96), and assume a short code ($G = N$) so that each data symbol is spread by the same sequence. Furthermore, assume that the same spreading sequence is used on the in-phase and quadrature components of the modulated carrier such that

$$h(t) = h_{I,n}(t) = h_{Q,n}(t) = \sum_{k=0}^{G-1} a_k u_{T_c}(t - kT_c). \tag{9.99}$$

It follows that

$$\begin{aligned} I_I &= \cos(\theta)\frac{1}{NT_c}\int_0^{NT_c}\sum_{k=0}^{N-1} a_k u_{T_c}(t-kT_c)\Big(\cos(2\pi\Sigma_f t) + \cos(2\pi\Delta_f t)\Big)\mathrm{d}t \\ &\quad - \sin(\theta)\frac{1}{NT_c}\int_0^{NT_c}\sum_{k=0}^{N-1} a_k u_{T_c}(t-kT_c)\Big(\sin(2\pi\Sigma_f t) + \sin(2\pi\Delta_f t)\Big)\mathrm{d}t \\ &= \frac{1}{N}\sum_{k=0}^{N-1} a_k\left(\cos(\theta)\int_k^{k+1}\Big(\cos(2\pi\Sigma_f T_c t) + \cos(2\pi\Delta_f T_c t)\Big)\mathrm{d}t\right. \\ &\quad \left. - \sin(\theta)\int_k^{k+1}\Big(\sin(2\pi\Sigma_f T_c t) + \sin(2\pi\Delta_f T_c t)\Big)\mathrm{d}t\right). \end{aligned} \tag{9.100}$$

Likewise,

$$\begin{aligned} I_Q &= \frac{1}{N}\sum_{k=0}^{N-1} a_k\left(\cos(\theta)\int_k^{k+1}\Big(\sin(2\pi\Delta_f T_c t) - \sin(2\pi\Sigma_f T_c t)\Big)\mathrm{d}t\right. \\ &\quad \left. + \sin(\theta)\int_k^{k+1}\Big(\cos(2\pi\Delta_f T_c t) - \sin(2\pi\Sigma_f T_c t)\Big)\mathrm{d}t\right). \end{aligned} \tag{9.101}$$

Fortunately, the above integrals exist in closed form. Defining

$$\alpha \triangleq 2\pi\Sigma_f T_c \tag{9.102}$$

$$\beta \triangleq 2\pi\Delta_f T_c \tag{9.103}$$

yields

$$I_I = \frac{1}{N}\sum_{k=0}^{N-1} a_k \left(\cos(\theta)\left(\frac{\sin((k+1)\alpha)-\sin(k\alpha)}{\alpha}+\frac{\sin((k+1)\beta)-\sin(k\beta)}{\beta}\right)\right.$$
$$\left.-\sin(\theta)\left(\frac{\cos(k\alpha)-\cos((k+1)\alpha)}{\alpha}+\frac{\cos(k\beta)-\cos((k+1)\beta)}{\beta}\right)\right) \tag{9.104}$$

and

$$I_Q = \frac{1}{N}\sum_{k=0}^{N-1} a_k \left(\cos(\theta)\left(\frac{\cos(k\beta)-\cos((k+1)\beta)}{\beta}-\frac{\cos(k\alpha)-\cos((k+1)\alpha)}{\alpha}\right)\right.$$
$$\left.+\sin(\theta)\left(\frac{\sin((k+1)\beta)-\sin(k\beta)}{\beta}-\frac{\cos(k\alpha)-\cos((k+1)\alpha)}{\alpha}\right)\right). \tag{9.105}$$

Due to the random phase of the CW tone interferer, the CW tone interference is circularly symmetric similar to AWGN. This allows us to rotate the signal constellation for the purpose of calculating the bit error probability. The rotated constellation is shown in Fig. 9.16. In the absence of CW tone interference, the probability of correct symbol reception is

$$P[c] = (1-P_b)^2, \tag{9.106}$$

where

$$P_b = Q\left(\sqrt{2\gamma_b}\right) \tag{9.107}$$

is the bit error probability, and $\gamma_b = E_b/N_o$ is the received bit energy-to-noise ratio.

When CW tone interference is present, the probability of correct reception is

$$P_{C|b_0b_1} = (1-P_{b1})(1-P_{b2}). \tag{9.108}$$

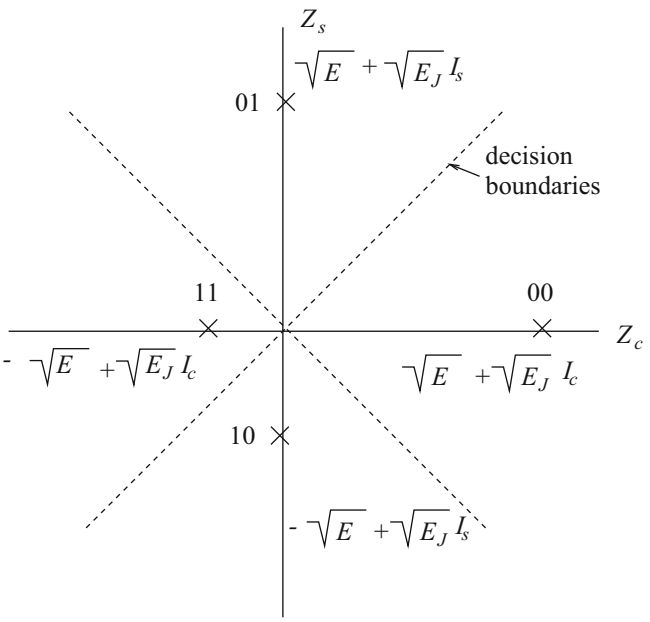

Fig. 9.16 QPSK signal constellation with tone interference

Observe that the error probability depends on the transmitted symbol and the interference impairment I_I and I_Q. Referring to Fig. 9.16

$$P_{C|00} = (1 - P_{b1})(1 - P_{b2}) \tag{9.109}$$

where

$$P_{b1} = P_{b2} = Q\left(\sqrt{\frac{2E_b}{N_o}\left(1 + 2\sqrt{E_J/E}I_I + (E_J/E)^2 I_I^2\right)}\right). \tag{9.110}$$

Hence,

$$P_{b|00} = Q\left(\sqrt{\frac{2E_b}{N_o}\left(1 + 2\sqrt{E_J/E}I_I + (E_J/E)^2 I_I^2\right)}\right). \tag{9.111}$$

In a similar fashion,

$$P_{b|01} = Q\left(\sqrt{\frac{2E_b}{N_o}\left(1 + 2\sqrt{E_J/E}I_Q + (E_J/E)^2 I_Q^2\right)}\right) \tag{9.112}$$

$$P_{b|11} = Q\left(\sqrt{\frac{2E_b}{N_o}\left(1 - 2\sqrt{E_J/E}I_I + (E_J/E)^2 I_I^2\right)}\right) \tag{9.113}$$

$$P_{b|10} = Q\left(\sqrt{\frac{2E_b}{N_o}\left(1 - 2\sqrt{E_J/E}I_Q + (E_J/E)^2 I_Q^2\right)}\right). \tag{9.114}$$

Since all symbols are equally likely, the bit error probability is

$$P_b = \frac{1}{4}(P_{b|00} + P_{b|11} + P_{b|10} + P_{b|01}). \tag{9.115}$$

Observe that the bit error probability depends on I_I and I_Q. However I_I and I_Q are random variables due to the random phase θ. Therefore, the bit error probability must be calculated by averaging (9.115) over random phase of the CW tone interferer.

Figure 9.17 shows the bit error probability when the length-15 m-sequence $\mathbf{a}^{(2)}$ in (9.73) is used as a short code ($G = 15$). Figure 9.17 arbitrarily assumes that $f_c = 280\,\text{MHz}$, and $T_c = 191 \times 10^{-9}\,\text{s}$. Observe that the bit error probability varies greatly with the frequency of the CW tone interferer. It is interesting to note that an interfering tone placed at the carrier frequency f_c does not give the worst case performance. Also, the bit error probability is seen to exhibit an error floor due to the AWGN.

Figure 9.18 shows the bit error probability when the length-11 Barker sequence $\mathbf{a}^{(1)}$ in (9.73) is used as a short code ($G = 11$). Observe that the length-11 Barker sequence generally has worse performance for the same E/E_J than the length-15 m-sequence, except at frequencies where the length-15 m-sequence is highly sensitive to tone interference. This is because the length-11 Barker sequence has a lower processing gain compared to the length-15 m-sequence.

Figure 9.19 inverts Fig. 9.17 and plots the E/E_J required to achieve a bit error rate of 10^{-6} with the length-15 m-sequence in the presence of a CW tone interferer and AWGN. Likewise, Fig. 9.20 inverts Fig. 9.18 for the length-11 Barker sequence. Observe that the sensitivity to CW tone interference is much less with the Barker sequence.

The sensitivity of the error probability to the frequency of the tone interferer can be explained as follows. The data symbols on the in-phase and quadrature channels are spread by using the amplitude shaping pulse

$$h(t) = \sum_{k=0}^{N-1} a_k h_c(t - kT_c), \tag{9.116}$$

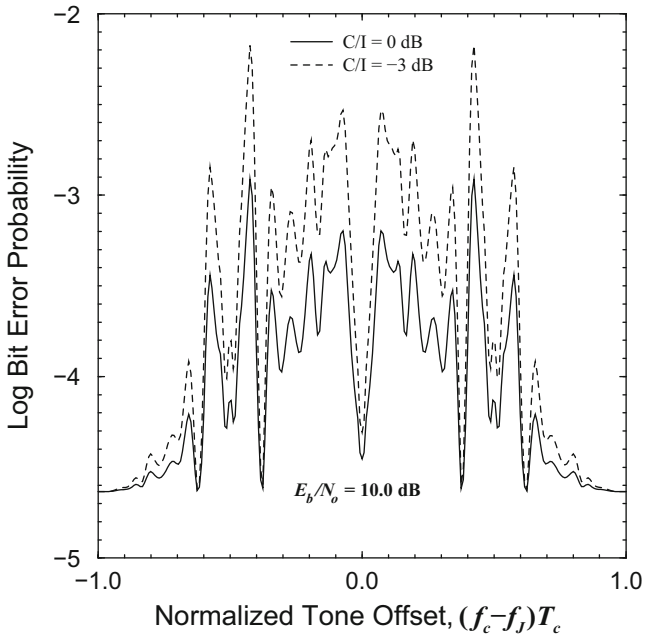

Fig. 9.17 Bit error probability with length-15 *m*-sequence

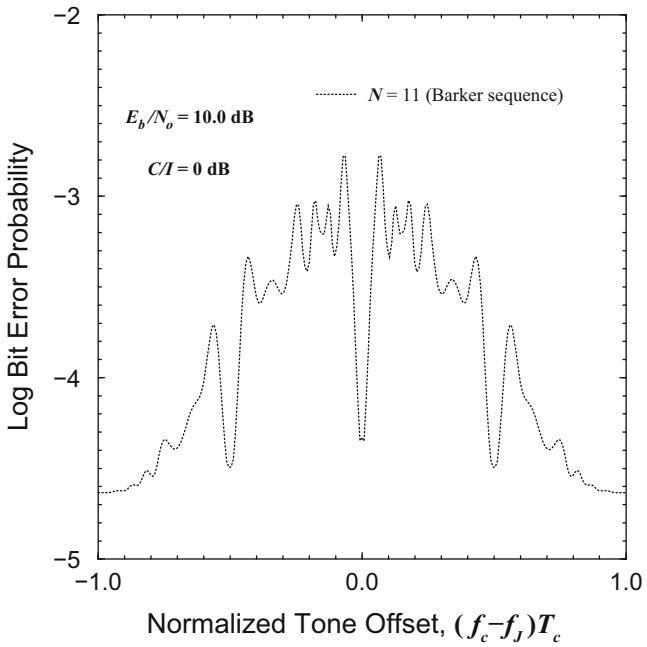

Fig. 9.18 Bit error probability with the length-11 Barker sequence

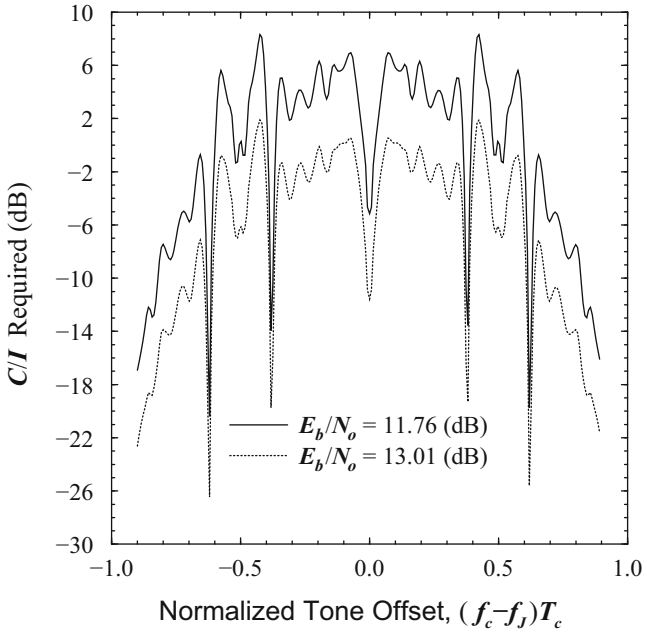

Fig. 9.19 Required C/I to achieve 10^{-6} bit error rate with a length-15 *m*-sequence

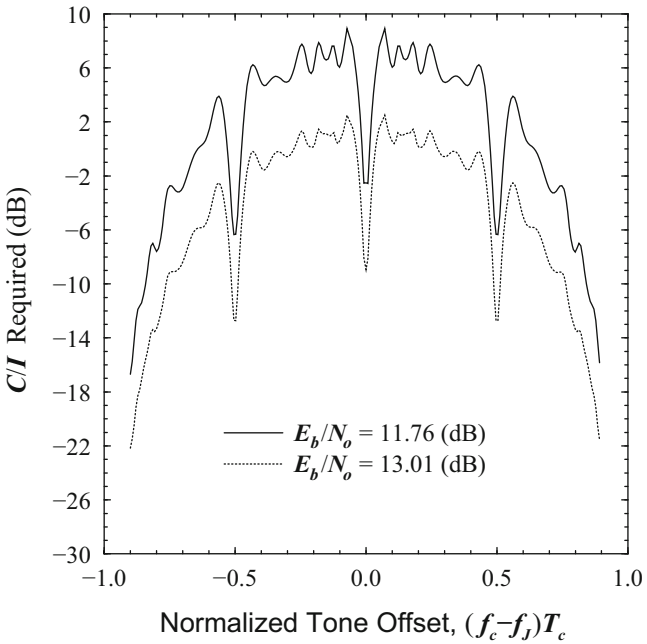

Fig. 9.20 Required C/I to achieve 10^{-6} bit error rate with a length-11 Barker sequence

where $\{a_k\}_{k=0}^{N-1}$ is the periodic spreading sequence of length N. After quadrature demodulation, the receiver employs a correlator or matched filter detector having the impulse response[4]

$$\begin{aligned} h_r(t) &= h^*(NT_c - t) \\ &= \sum_{k=0}^{N-1} a_{N-k} h_c(t - kT_c). \end{aligned} \tag{9.117}$$

The filter $h_r(t)$ has transfer function

$$\begin{aligned} H_r(f) &= \int_{-\infty}^{\infty} h_r(t) \mathrm{e}^{-j2\pi ft} \mathrm{d}t \\ &= \int_{-\infty}^{\infty} \sum_{k=0}^{N-1} a_{N-k} h_c(t - kT_c) \mathrm{e}^{-j2\pi ft} \mathrm{d}t \\ &= \sum_{k=0}^{N-1} a_{N-k} \int_{-\infty}^{\infty} h_c(t - kT_c) \mathrm{e}^{-j2\pi ft} \mathrm{d}t \\ &= H_c(f) \sum_{k=0}^{N-1} a_{N-k} \mathrm{e}^{-j2\pi fkT_c} \\ &= H_c(f) A(f), \end{aligned} \tag{9.118}$$

where

$$A(f) = \sum_{k=0}^{N-1} a_{N-k} \mathrm{e}^{-j2\pi fkT_c}. \tag{9.119}$$

For a rectangular chip shaping function $h_c(t) = u_{T_c}(t)$,

$$H_c(f) = \mathrm{sinc}(fT_c) \mathrm{e}^{-j\pi fT_c}. \tag{9.120}$$

The corresponding amplitude response $|H_r(f)|$ for the length-15 m-sequence and the length-11 Barker sequence is identical in form to the corresponding transmitted psds shown in Figs. 9.14 and 9.13, respectively. The frequencies where $|H_r(f)|$ has the highest relative gain are the exact same frequencies where the CW tone interferer causes a large error probability. If the length of the short code is increased, the sensitivity to CW tone interference will not necessarily diminish. To make the receiver less sensitive to CW tone interference, the aperiodic autocorrelation function in (9.21) should be as close to ideal as possible. In other words, the power spectrum $\Phi_{k,k}(f)$ defined in (9.69) is as flat as possible. Although some types of sequences, such as Gold and Kasami sequences, have excellent cross-correlation properties, their aperiodic autocorrelation functions are usually far from ideal resulting in a power spectrum $\Phi_{k,k}(f)$ is typically full of peaks and nulls. The Barker sequences have the best aperiodic autocorrelation properties for a given sequence length N when they exist, and will result in the least sensitivity to tone interference.

9.4.2 Short Code Design

Sometimes it is desirable to construct short sequences of a given sequence length N that have good aperiodic autocorrelation properties with a corresponding power spectrum that is a flat as possible. One possibility is to design such sequences based on a MMSE criterion baaed on their aperiodic autocorrelation function in (9.21). The ideal aperiodic autocorrelation function

[4]The usual case is assumed, where $h_c(-t) = h_c(t)$.

is the perfect "thumb-tack" function $\phi_{k,k}^{a\ (\text{ideal})}(n) = \delta(n)$. In this case, the discrete-time Fourier transform of $\phi_{k,k}^{a\ (\text{ideal})}(n)$ gives the flat power spectrum $\Phi^a(f) = 1$. However, spreading codes having ideal aperiodic autocorrelation functions do not exist for any length. Here, short spreading sequences are designed to minimize the mean square error

$$\varepsilon = \frac{1}{N}\sum_{n=0}^{N-1}\left(\phi_{k,k}^a(n) - \phi_{k,k}^{a\ (\text{ideal})}(n)\right)^2 \tag{9.121}$$

$$= \frac{1}{N}\sum_{n=1}^{N-1}\left(\phi_{k,k}^a(n)\right)^2, \tag{9.122}$$

where the summation may be started at $n = 1$ since $\phi_{k,k}^a(0) = 1$ for any sequence. Unfortunately, there is no easy analytical method to find such sequences. However, for relatively small N the sequences can be found by an exhaustive search. For sequence lengths $N = 2, 3, 4, 5, 7, 11$ and 13, the above process will generate the Barker sequences in Sect. 9.2.5, along with their mirror images (time reversed sequences). So the Barker sequences are optimal in a minimum mean square sense.

Example 9.2. Suppose our objective is to find MMSE binary spreading sequences of length $N = 15$. In this case, the following four sequences will minimize the mean square error in (9.122):

$$\mathbf{x}_1 = \{-1-1-1-1-1+1+1-1-1+1+1-1+1-1+1\}$$
$$\mathbf{x}_2 = \{+1-1+1-1+1+1-1-1+1+1-1-1-1-1-1\}$$
$$\mathbf{x}_3 = \{-1-1-1+1+1+1-1+1+1+1-1+1+1-1+1\}$$
$$\mathbf{x}_4 = \{+1-1+1+1-1+1+1+1-1+1+1+1-1-1-1\}$$

Observe that $\mathbf{x}_1$ and $\mathbf{x}_3$ are the mirror images (time reversals) of $\mathbf{x}_2$ and $\mathbf{x}_4$, respectively. The aperiodic autocorrelation function for all four sequences is identical and the scaled version $N\phi^a(n)$ is plotted in Fig. 9.21. Each sequence has $\varepsilon = 1$ with a maximum "off-peak" aperiodic autocorrelation value equal to $\max_n N\phi^a(n) = 3$.

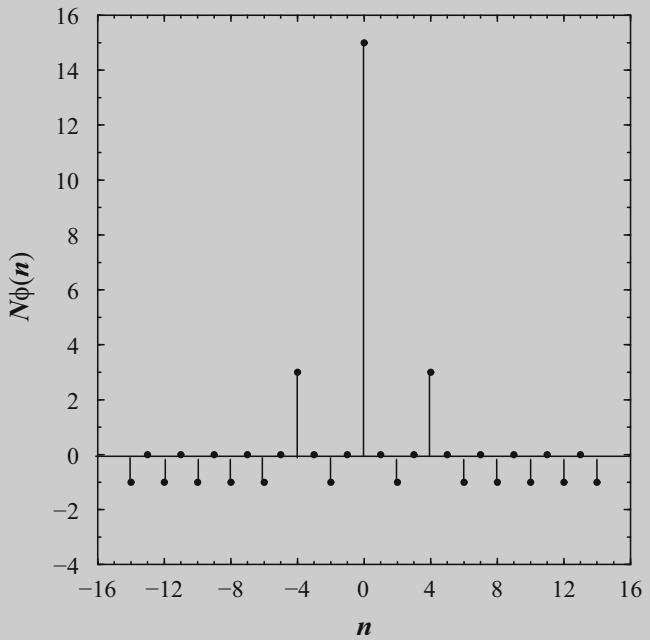

Fig. 9.21 Aperiodic autocorrelation for optimized length-15 sequences

(continued)

Example 9.2 (continued)

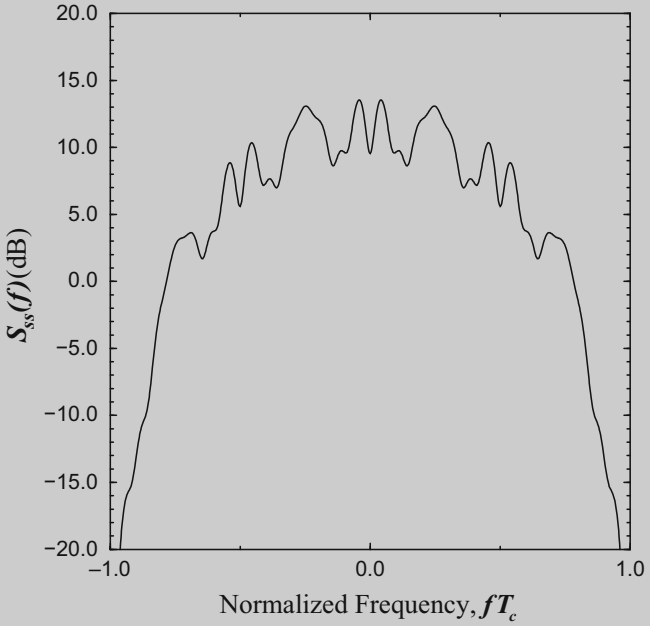

Fig. 9.22 Power spectrum with optimized length-15 sequences

The corresponding power spectral density achieved with these sequences is shown in Fig. 9.22 for the case of rectangular chip shaping, $h_c(t) = u_{T_c}(t)$. Note that the power spectrum exhibits considerably less variation than that corresponding to the length-15 m-sequence in Fig. 9.14, but is not as good as that corresponding to the length-11 Barker sequence in Fig. 9.13.

9.4.3 Long Code

With a long code each data symbol is spread with a subsequence of a long PN sequence. In this case, the error probability must be averaged over the starting phase of the PN subsequence that is used to spread each data symbol.

Figure 9.23 shows the effect of using a long PN sequence. Three cases are considered; a length-31 m sequence with generator polynomial $1 + x^2 + x^5$, a length-127 m-sequence with generator polynomial $1 + x + x^7$, and a length-2047 m-sequence with generator polynomial $1 + x + x^{11}$. Figure 9.24 shows the length-63 m-sequence with generator polynomial $1 + x + x^6$. The processing gain in each case is $G = 15$ chips/symbol. For the length-63 m-sequence, 15 and 63 have a common factor of 3 and, therefore, there are three different sets of subsequences to consider.

Observe that the bit error probability with a long code is less sensitive to the CW tone frequency as compared to a short code. For sequence lengths of 127 and 2047, the bit error probability is maximized when $f_J = f_c$. For all three sequence lengths, there are still some spectral irregularities, because the length of the shift register (5, 7, and 11) that is used to generate the PN sequence is less than the processing gain (15). Hence, the data symbols are not spread with all possible binary N-tuples, thus leading to the irregularities observed in Fig. 9.23. It is interesting to note that the length-2047 m-sequence seems to be more sensitive to an interfering tone at the carrier frequency than the length-127 m-sequence. The reason is that the length-15 subsequences of the length-127 m-sequence tend to be more balanced (equal number of -1's and 1's) than the length-15 subsequences of the length-2047 m-sequence.

Finally, comparison of Figs. 9.17 and 9.23 leads to the observation that the bit error probability with the short length-15 PN sequence is worse than that realized with a long PN sequence (e.g., the length-127 m-sequence) with a processing gain of 15 only over 4 narrow ranges of interfering tone frequencies.

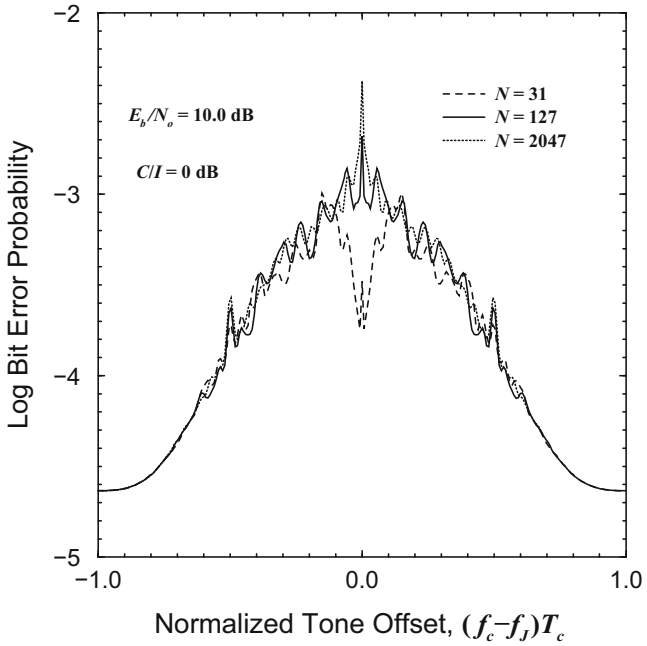

Fig. 9.23 Bit error probability with length-31, 127, and 2047 *m*-sequences

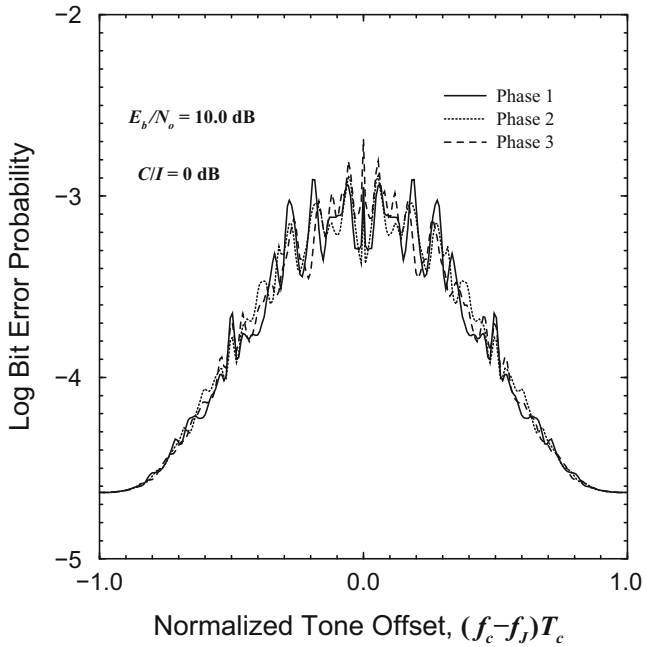

Fig. 9.24 Bit error probability with length-63 *m*-sequence

9.5 DS Spread Spectrum on Frequency-Selective Fading Channels

Suppose that the DS complex envelope $\tilde{s}(t)$ is strictly bandlimited to a bandwidth of $W/2$ Hz by using, for example, root-raised cosine pulse shaping. Since the low-pass signal $\tilde{s}(t)$ is band-limited to $|f| \leq W/2$, the sampling theorem can be invoked and $\tilde{s}(t)$ can be completely described by the set of complex samples $\{\tilde{s}(n/W)\}_{n=-\infty}^{\infty}$. The sampled version of $\tilde{s}(t)$ is

$$\tilde{s}_\delta(t) = \sum_{n=-\infty}^{\infty} \tilde{s}\left(\frac{n}{W}\right)\delta\left(t-\frac{n}{W}\right) \tag{9.123}$$

$$= \tilde{s}(t)\sum_{n=-\infty}^{\infty}\delta\left(t-\frac{n}{W}\right). \tag{9.124}$$

Taking the Fourier transform of both sides of (9.124) gives

$$\begin{aligned}\tilde{S}_\delta(f) &= \tilde{S}(f) * W\sum_{n=-\infty}^{\infty}\delta(f-nW)\\ &= W\sum_{n=-\infty}^{\infty}\tilde{S}(f)*\delta(f-nW)\\ &= W\sum_{n=-\infty}^{\infty}\tilde{S}(f-nW).\end{aligned} \tag{9.125}$$

From (9.125),

$$\tilde{S}(f) = \frac{1}{W}\tilde{S}_\delta(f)\,,\quad 0\le|f|\le W/2. \tag{9.126}$$

Another useful expression can be obtained by taking the Fourier transform of both sides of (9.123) giving

$$\tilde{S}_\delta(f) = \sum_{n=-\infty}^{\infty}\tilde{s}\left(\frac{n}{W}\right)\mathrm{e}^{-j2\pi nf/W}. \tag{9.127}$$

Combining (9.126) and (9.127) gives

$$\tilde{S}(f) = \frac{1}{W}\sum_{n=-\infty}^{\infty}\tilde{s}\left(\frac{n}{W}\right)\mathrm{e}^{-j\pi nf/W}\,,\quad 0\le|f|\le W/2. \tag{9.128}$$

If the low-pass signal $\tilde{s}(t)$ is transmitted over a multipath-fading channel with time-variant transfer function $T(f,t)$, the received (noiseless) complex envelope is

$$\tilde{r}(t) = \int_{-\infty}^{\infty}\tilde{S}(f)T(f,t)\mathrm{e}^{j2\pi ft}\mathrm{d}f. \tag{9.129}$$

Substituting $\tilde{S}(f)$ from (9.128) gives

$$\begin{aligned}\tilde{r}(t) &= \frac{1}{W}\sum_{n=-\infty}^{\infty}\tilde{s}\left(\frac{n}{W}\right)\int_{-\infty}^{\infty}T(f,t)\mathrm{e}^{-j2\pi f(t-n/W)}\mathrm{d}f\\ &= \frac{1}{W}\sum_{n=-\infty}^{\infty}\tilde{s}\left(\frac{n}{W}\right)g\left(t-\frac{n}{W},t\right)\\ &= \frac{1}{W}\sum_{n=-\infty}^{\infty}\tilde{s}\left(t-\frac{n}{W}\right)g\left(\frac{n}{W},t\right),\end{aligned} \tag{9.130}$$

where $g(\tau,t)$ is the time-variant impulse response of the channel. By defining

$$g_n(t) = \frac{1}{W}g\left(\frac{n}{W},t\right) \tag{9.131}$$

the noiseless received complex envelope can be written as

$$\tilde{r}(t) = \sum_{n=-\infty}^{\infty} g_n(t)\tilde{s}\left(t - \frac{n}{W}\right) \tag{9.132}$$

and it follows that the complex low-pass impulse response of the channel is

$$g(t,\tau) = \sum_{n=-\infty}^{\infty} g_n(t)\delta\left(\tau - \frac{n}{W}\right). \tag{9.133}$$

For WWSUS channels, the $\{g_n(t)\}$ in (9.131) are independent complex Gaussian random processes. For all practical purposes, the channel will be causal with an impulse response that is non-zero over a time interval of duration $T_{\max}$. In this case, $g_n(t) = 0,\ n \le 0, n > L$, where $L = \lfloor T_{\max}/W \rfloor + 1$ and $\lfloor x \rfloor$ is the smallest integer greater than x. It follows that the channel impulse response is

$$g(t,\tau) = \sum_{n=1}^{L} g_n(t)\delta\left(\tau - \frac{n}{W}\right). \tag{9.134}$$

In conclusion, the frequency-selective fading channel can be modeled as an L-tap, $1/W$-spaced, tapped delay line with tap gain vector

$$\mathbf{g}(t) = (g_1(t), g_2(t), \ldots, g_L(t))$$

as shown in Fig. 9.25. It should be emphasized that the channel vector $\mathbf{g}(t)$ is *not* the same as the channel vector $\mathbf{g}_T(t)$ associated with the T-spaced discrete-time white noise channel model in Sect. 2.5.6.

If ideal Nyquist chip amplitude pulse shaping is used such that $h_c(t) = \text{sinc}(t/T_c)$, then $W = 1/T_c$ and the channel can be represented as a T_c-spaced or chip-spaced tapped delay line. Such a model is very convenient because it leads to a simplified analysis. However, if any other pulse shape is used, such as a root-raised cosine pulse, then the tapped delay line channel model in Fig. 9.25 is not T_c-spaced, e.g., a root-raised cosine pulse with $\beta = 1$ (or 100% excess bandwidth) results a $T_c/2$-spaced tapped delay line. Moreover, the $1/W$-spaced tapped delay line model was derived under the assumption of a strictly band-limited (non-causal) chip shaping pulse $h_c(t)$. Any time-limited (causal) chip shaping pulse leads to a spectrum $\tilde{S}(f)$ that is not band-limited and, therefore, the underlying assumptions in deriving the $1/W$-spaced tapped delay line model are violated. Very often, the channel is approximated as consisting of uncorrelated T_c-spaced rays, i.e.,

$$g(t,\tau) = \sum_{n=-\infty}^{\infty} g_n(t)\delta\left(\tau - nT_c\right). \tag{9.135}$$

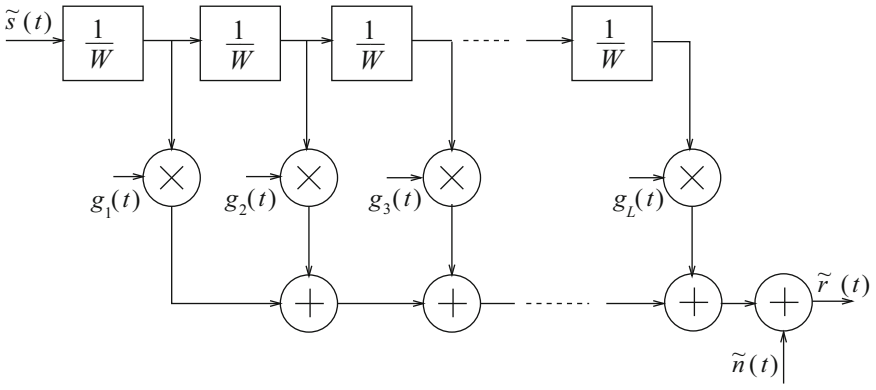

Fig. 9.25 Tapped delay line model of a frequency-selective fading channel, from [272]

9.5.1 RAKE Receiver

A variety of receiver structures can be used to detect DS spread spectrum signals. For DS CDMA where multiple users share the same band, there are two broad types of detectors. The first is a conventional correlator or matched filter detector. With a conventional detector the other user interference, or multiple-access interference, is treated as additional unwanted noise. The second is a multiuser detector, that uses co-channel demodulation to simultaneously detect all the signals that are present. This section concentrates on conventional detectors for DS spread spectrum signaling on multipath-fading channels.

A simple type of conventional detector uses the autocorrelation properties of the spreading sequences to reject the multipath interference [136, 137]. Sometimes this is called a multipath rejection receiver. Another approach is to exploit the autocorrelation properties of the spreading sequences to resolve the multipath components and combine them together to obtain a diversity advantage. Since the diversity is obtained from the multipath channel it is sometimes called multipath diversity.

To develop the multipath diversity receiver, suppose that one of M possible waveforms having complex envelopes $\tilde{s}_m(t), m = 0, \ldots, M-1$ are transmitted at each baud epoch. With the frequency-selective fading channel shown in Fig. 9.25, the corresponding received complex envelope is

$$\tilde{r}(t) = \sum_{\ell=1}^{L} g_\ell(t)\tilde{s}_m\left(t - \frac{\ell}{W}\right) + \tilde{n}(t) = \hat{s}_m(t) + \tilde{n}(t) \tag{9.136}$$

where

$$\hat{s}_m(t) = \sum_{\ell=1}^{L} g_\ell(t)\tilde{s}_m\left(t - \frac{\ell}{W}\right). \tag{9.137}$$

As discussed in Sect. 5.2, the maximum likelihood coherent receiver employs a correlator or matched filter to the possible received pulses $\hat{s}_m(t)$ to compute the metrics

$$\begin{aligned}\mu(m) &= \mathrm{Re}\left\{\int_0^T \tilde{r}(t)\hat{s}_m^*(t)\mathrm{d}t\right\} - E_{\hat{m}} \\ &= \mathrm{Re}\left\{\int_0^T \tilde{r}(t)\sum_{\ell=1}^{L} g_\ell^*(t)\tilde{s}_m^*(t-\ell/W)\mathrm{d}t\right\} - E_{\hat{m}},\end{aligned} \tag{9.138}$$

where $E_{\hat{m}}$ is energy in the received pulse $\hat{s}_m(t)$. The receiver chooses the index m that maximizes $\mu(m)$.

The receiver described by (9.138) correlates the received complex envelope $\tilde{r}(t)$ with delayed versions of the possible waveforms $\tilde{s}_m(t)$, followed by maximal ratio combining. This leads to the receiver structure shown in Fig. 9.26. By changing the variable of integration in (9.138) an alternate form of the RAKE receiver can be obtained as shown in Fig. 9.27. In this case the waveform $\tilde{s}_m(t)$ is correlated with delayed versions of the received complex envelope $\tilde{r}(t)$. The receivers in Figs. 9.26 and 9.27 were first derived by Price and Green [270], and are commonly called RAKE receivers due to their function and resemblance to an ordinary garden rake.

9.5.2 Error Probability of DS/BPSK with a RAKE Receiver

Consider DS/BPSK signaling with a short PN code ($G = N$). The two possible DS/BPSK waveforms that are transmitted at each baud epoch have the complex envelopes

$$\tilde{s}_0(t) = -\tilde{s}_1(t) = Ah(t), \tag{9.139}$$

where

$$h(t) = \sum_{k=0}^{N-1} a_k h_c(t - nT_c). \tag{9.140}$$

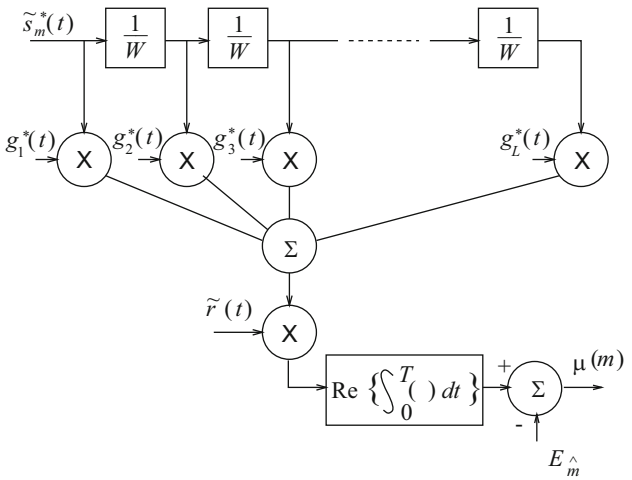

Fig. 9.26 RAKE receiver for DS/QPSK signals

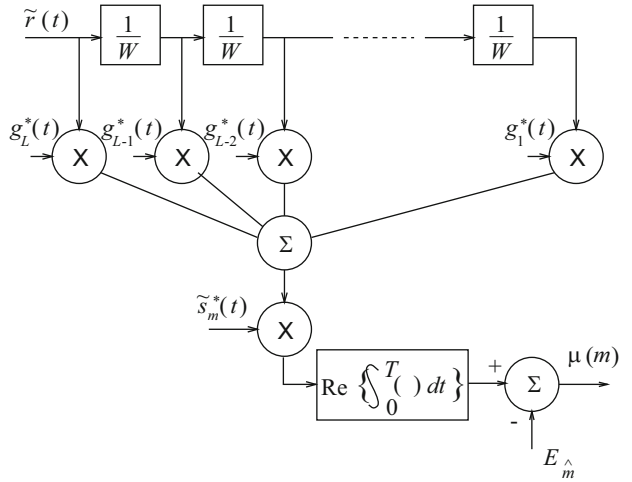

Fig. 9.27 Alternate form of RAKE receiver for DS/QPSK signals

With DS/BPSK the received waveforms $\hat{s}_m(t)$ have equal energy so the bias term $E_{\hat{m}}$ in (9.138) is not needed. Assume that $\tilde{s}_0(t)$ is transmitted. Then using (9.138)

$$\mu = \sum_{m=1}^{L}\sum_{\ell=1}^{L} \mathrm{Re}\left\{ g_m g_\ell^* \int_0^T \tilde{s}_0(t-m/W)\tilde{s}_0^*(t-\ell/W)\mathrm{d}t \right\} + \tilde{n}, \tag{9.141}$$

where

$$\tilde{n} = \sum_{m=1}^{L} \mathrm{Re}\left\{ g_m^* \int_0^T \tilde{n}(t)\tilde{s}_0^*(t-m/W)\mathrm{d}t \right\} \tag{9.142}$$

and $g_m = \alpha_m e^{j\phi_m}$. The random variable $\tilde{n}$ is Gaussian with zero mean and variance

$$\sigma_{\tilde{n}}^2 = 2EN_o \sum_{m=1}^{L} \alpha_m^2. \tag{9.143}$$

In general, the integral in (9.141) is a complicated function of the spreading sequence and chip amplitude shaping pulse that is used. However, certain cases lead to useful insight. For example, suppose the ideal Nyquist pulse $h_c(t) = \text{sinc}(t/T_c)$ with bandwidth $W = 1/T_c$ is used. Strictly speaking this pulse is non-causal so the limits of integration in (9.141) must be from $-\infty$ to ∞. This leads to[5]

$$\begin{aligned} I &\equiv \int_{-\infty}^{\infty} \tilde{s}_0(t - m/W)\tilde{s}_0^*(t - \ell/W)\mathrm{d}t \\ &= A^2 \sum_{k=0}^{N-1}\sum_{j=0}^{N-1} a_k a_j \int_{-\infty}^{\infty} h_c(t - (m+k)T_c)h_c(t - (\ell + j)T_c)\mathrm{d}t \\ &= A^2 \sum_{k=0}^{N-1} a_k a_{m+k-\ell} \int_{-\infty}^{\infty} h_c^2(t)\mathrm{d}t \\ &= 2E_c N\phi_{aa}(m-\ell) = 2E\phi_{aa}(m-\ell) \end{aligned} \tag{9.144}$$

where the second last step follows under the assumption of a short code. Therefore, (9.141) becomes

$$\mu = 2E\sum_{m=1}^{L}\alpha_m^2 + 2E\sum_{m=1}^{L}\sum_{\substack{\ell=1 \\ \ell\neq m}}^{L} \text{Re}\left\{g_m g_\ell^*\right\}\phi_{aa}(m-\ell) + \tilde{n}. \tag{9.145}$$

The second term in the above expression is a self-interference that arises from the non-ideal autocorrelation properties of the spreading sequence.

To demonstrate the effect of the self-interference, assume a WSSUS Rayleigh fading channel and consider the random variable

$$\begin{aligned} Y_{m,\ell} &= \text{Re}\left\{g_m g_\ell^*\right\} \\ &= \alpha_m \cos(\phi_m)\alpha_\ell \cos(\phi_\ell) + \alpha_m \sin(\phi_m)\alpha_\ell \sin(\phi_\ell). \end{aligned} \tag{9.146}$$

Define the new random variables

$$X_{I,k} = \alpha_k \cos(\phi_k) \qquad X_{Q,k} = \alpha_k \sin(\phi_k). \tag{9.147}$$

Then

$$\alpha_k = \sqrt{X_{I,k}^2 + X_{Q,k}^2} \qquad \phi_k = \text{Tan}^{-1}\frac{X_{I,k}}{X_{Q,k}}. \tag{9.148}$$

Therefore,

$$Y_{m,\ell} = X_{I,m}X_{I,\ell} + X_{I,m}X_{I,\ell}. \tag{9.149}$$

Since the $X_{I,k}$ and $X_{I,k}$ are independent zero-mean Gaussian random variables with variance σ_k^2, $Y_{m,\ell}$ has the Laplacian density

$$p_{Y_{m,\ell}}(y) = \frac{1}{2\sigma_m\sigma_\ell}\exp\left\{-\frac{|y|}{\sigma_m\sigma_\ell}\right\}. \tag{9.150}$$

Making the substitution for $Y_{m,\ell}$ and rearranging the sum in the second term in (9.145) gives

$$\mu = 2E\sum_{m=1}^{L}\alpha_m^2 + 4E\sum_{k=1}^{L-1}\sum_{i=1}^{L-1-k} Y_{i,i+k}\phi_{aa}(k) + \tilde{n}. \tag{9.151}$$

[5] Since DS/BPSK signaling is used the spreading sequence $\mathbf{a}$ is real with autocorrelation function $\phi_{aa}(n) = \text{E}[a_i a_{i+n}]$.

It is difficult to evaluate the effect of the self-interference exactly, because the $Y_{m,\ell}$ are non-Gaussian and correlated. However, the self-interference due to multipath can be minimized by using spreading codes that have small autocorrelation sidelobes in the time intervals during which delayed signals with significant power are expected. For large delays, the stringent requirements on the autocorrelation function can be relaxed. For asynchronous CDMA applications, the spreading codes still must have small cross-correlation sidelobes over all delays. It is easy to find reasonably large sets of sequences that satisfy these properties. For example, a set of $2^m + 1$ Gold sequences can be generated of length $2^m - 1$. Of these $2^m + 1$ sequences, $2^{m-n+1} + 1$ will have their first autocorrelation off-peak ($t_m - 2$ or t_m) at least n chip durations from the main autocorrelation peak. Consequently, these $2^{m-n+1} + 1$ sequences will introduce negligible self-interference if they are used on channels having impulse responses up to nT_c seconds long.

If the spreading sequences have an ideal autocorrelation function, i.e., $\phi_{aa}(n-m) = \delta_{nm}$, then there is no self-interference and (9.151) becomes

$$\mu = 2E \sum_{m=1}^{L} \alpha_m^2 + \tilde{n}. \tag{9.152}$$

Under this condition, the probability of bit error is

$$P_b(\gamma_b) = Q\left(\sqrt{2\gamma_b}\right), \tag{9.153}$$

where γ_b is the received bit energy-to-noise ratio given by

$$\gamma_b = \frac{1}{\sigma_{\tilde{n}}^2}\left(2E \sum_{m=1}^{L} \alpha_m^2\right)^2 = \sum_{m=1}^{L} \gamma_m \tag{9.154}$$

where

$$\gamma_m = \frac{\alpha_m^2 E}{N_o}. \tag{9.155}$$

With Rayleigh fading, each of the γ_m is exponentially distributed with density function

$$p(\gamma_m) = \frac{1}{\bar{\gamma}_m} \exp\left\{-\frac{\gamma_m}{\bar{\gamma}_m}\right\}, \tag{9.156}$$

where $\bar{\gamma}_m$ is the average received bit energy-to-noise ratio for the kth channel tap. To compute the density of γ_b, first note that the characteristic function of γ_m is

$$\psi_{\gamma_m}(jv) = \frac{1}{1 - jv\bar{\gamma}_m} \tag{9.157}$$

so that the characteristic function of γ_b is

$$\psi_{\gamma_b}(jv) = \prod_{m=1}^{L} \frac{1}{1 - jv\bar{\gamma}_m}. \tag{9.158}$$

By using a partial fraction expansion and taking the inverse characteristic function, the density of γ_b is

$$p_{\gamma_b}(x) = \sum_{m=1}^{L} \frac{A_m}{\bar{\gamma}_m} \exp\left\{-\frac{x}{\bar{\gamma}_k}\right\}, \tag{9.159}$$

where

$$A_m = \prod_{\substack{i=1 \\ i \neq m}}^{L} \frac{\bar{\gamma}_m}{\bar{\gamma}_m - \bar{\gamma}_i}. \tag{9.160}$$

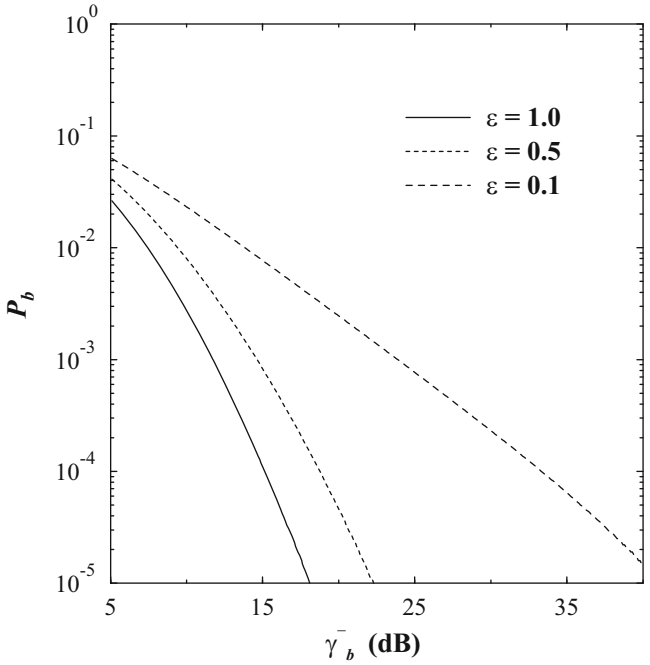

Fig. 9.28 Bit error probability with a RAKE receiver for DS/BPSK signaling on a multipath-fading channel. The channel has $L = 4$ taps and a 4-tap RAKE receiver is used

Therefore, with Rayleigh fading the average probability of bit error is

$$\begin{aligned} P_b &= \int_0^\infty Q\left(\sqrt{2x}\right) p_{\gamma_b}(x)\mathrm{d}x \\ &= \frac{1}{2}\sum_{m=1}^{L} A_m \left(1 - \sqrt{\frac{\bar{\gamma}_m}{1+\bar{\gamma}_m}}\right). \end{aligned} \tag{9.161}$$

In order to proceed further the $\bar{\gamma}_m$ must be specified. One plausible model assumes an exponentially decaying power-delay profile, e.g.,

$$\bar{\gamma}_m = C\mathrm{e}^{-k/\varepsilon}, \tag{9.162}$$

where ε controls the delay spread and C is chosen to satisfy the constraint $\sum_{m=1}^{L} \bar{\gamma}_m = \bar{\gamma}_b$. Solving for C yields

$$\bar{\gamma}_m = \frac{(1-\mathrm{e}^{-1/\varepsilon})\mathrm{e}^{-k/\varepsilon}}{\mathrm{e}^{-1/\varepsilon} - \mathrm{e}^{-(L+1)/\varepsilon}}\,\bar{\gamma}_b. \tag{9.163}$$

The probability of bit error is plotted in Fig. 9.28 for $L = 4$ and various values of ε. For small ε, the channel is not dispersive and very little multipath diversity is obtained. However, as ε becomes large the channel becomes more dispersive and a greater diversity gain is achieved.

Finally, the number of taps actually used in the RAKE receiver can be less than the channel length L. However, such a RAKE receiver will not capture all the received signal energy and will suffer from some loss in performance.

9.6 Error Probability for DS CDMA on AWGN Channels

DS CDMA systems achieve multiple-access capability by assigning each user a unique PN spreading sequence. In general, however, the transmissions from the different users are not synchronized and arrive at the intended receiver with different amplitudes, delays, and phases. The exact error probability with a conventional correlation detector will depend on the

particular spreading sequences that are employed and will also be a function of the random amplitudes, delays, and phases of the signals that arrive at the intended receiver. Unfortunately, the exact error probability is difficult to derive and evaluate and, therefore, a variety of upper and lower bounds, and Gaussian approximations to the probability of error have been suggested in the literature.

Suppose that K users simultaneously access the channel using DS/BPSK signaling with short spreading codes of length N. The transmitted complex envelope for the ith user is

$$\tilde{s}^{(i)}(t) = A \sum_n x_n^{(i)} h^{(i)}(t - nT) \tag{9.164}$$

where

$$h^{(i)}(t) = \sum_{k=0}^{N-1} a_k^{(i)} h_c(t - kT_c) \tag{9.165}$$

and $\mathbf{a}^{(i)} = \{a_k^{(i)}\}$ and $\mathbf{x}^{(i)} = \{x_n^{(i)}\}$ are the ith user's spreading and data sequences, respectively. A real-valued spreading sequence assumed with chips $a_k^{(i)}$ chosen from the set $\{-1, +1\}$, corresponding to simple binary spreading or dual channel quaternary spreading. The data symbols $x_n^{(i)}$ are independent, random variables chosen from the set $\{-1, +1\}$ with equal probability. In practice, the spreading sequences $\mathbf{a}^{(i)}$ are carefully chosen to have good correlation properties, e.g., Gold sequences or Kasami sequences.

With CDMA, the signals from the various MSs in a cell will arrive at the corresponding BS with different power levels. DS CDMA systems must be power controlled such that all signals arrive at the intended receiver with the same power level; otherwise, a large performance loss will result. Power control is needed to combat the near-far effect, where strong signals will capture the receiver and prevent detection of the weaker signals. The power control loop must be fast enough to compensate not only for path loss and shadowing, but envelope fading as well. Under the assumption of perfect power control and a frequency non-selective channel, the received complex envelope will be[6]

$$\tilde{r}(t) = \sum_{i=1}^{K} e^{j\phi_i} \tilde{s}^{(i)}(t - \tau_i) + \tilde{n}(t) \tag{9.166}$$

where the $\{\tau_i\}$ and $\{\phi_i\}$ are the random delays and carrier phases of the received signals. This leads to the model shown in Fig. 9.29.

This section considers the performance of an ideal correlation detector, where the composite received signal at a BS is multiplied by a synchronized and conjugated replica of the spreading sequence corresponding to a particular target MS whose data sequence is to be detected. Multiplication of a spreading sequence by a synchronized version of itself will despread the received signal corresponding to the particular target MS, while further spreading the received signals corresponding

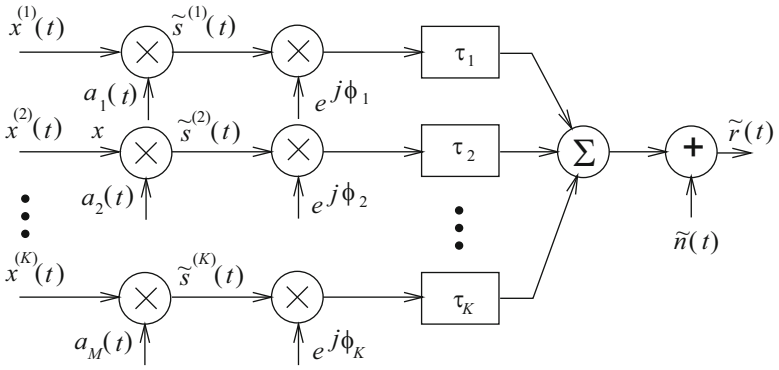

Fig. 9.29 DS CDMA signaling on a perfectly power controlled flat fading channel

[6]Here the normalization $\alpha = 1$ is assumed.

to other MSs in the composite received signal. As a result, the data sequence of the target MS can be obtained from the output of the correlator. Due to symmetry, only the decorrelator that recovers the data sequence from the first MS is considered. Furthermore, since only the relative delays and phases of the K signals comprising the composite received signal are important, it can be assumed that $\tau_1 = 0$ and $\phi_1 = 0$, while the remaining ϕ_i are uniformly distributed on $[0, 2\pi)$ and the remaining τ_i are uniformly distributed on $[0, T)$. Hence, it is assumed that the composite received signal at the BS is despread by multiplying by the spreading sequence $a^{(1)}(t)$.

The decision variable at the output of the correlator in Fig. 9.1 has been derived by Lehnert and Pursley [200] as

$$\mu_n = \sqrt{2E}\left[x_n^{(1)} + \sum_{k=2}^{K} B_{k,1}(x_n^{(k)}, x_{n-1}^{(k)}, \tau_k)\cos\phi_k\right] + \tilde{n}_I \tag{9.167}$$

where $\tilde{n}_I$ is a zero-mean complex Gaussian random variable with variance N_o

$$B_{k,1}(x_n^{(k)}, x_{n-1}^{(k)}, \tau_k) = x_{n-1}^{(k)} R_{k,1}^{p}(\tau_k) + x_n^{(k)} \hat{R}_{k,1}^{p}(\tau_k) \tag{9.168}$$

and $R_{k,m}^{p}(\tau)$ and $\hat{R}_{k,m}^{p}(\tau)$ are the continuous-time partial cross-correlation functions of $a^{(k)}(t)$ and $a^{(m)}(t)$, defined by

$$R_{k,m}^{p}(\tau) = \frac{1}{T}\int_0^{\tau} a^{(k)}(t-\tau)a^{(m)}(t)dt \tag{9.169}$$

$$\hat{R}_{k,m}^{p}(\tau) = \frac{1}{T}\int_{\tau}^{T} a^{(k)}(t-\tau)a^{(m)}(t)dt. \tag{9.170}$$

The functions $R_{k,m}^{p}(\tau)$ and $\hat{R}_{k,m}^{p}(\tau)$ can be expressed in terms of the discrete aperiodic cross-correlation function $\phi_{k,m}^{a}(n)$ and the continuous-time partial chip autocorrelation functions $R_h(\delta)$ and $\hat{R}_h(\delta)$ in (9.33) as

$$R_{k,m}^{p}(\tau) = \phi_{k,m}^{a}(\ell - N)\hat{R}_h(\delta) + \phi_{k,m}^{a}(\ell + 1 - N)R_h(\delta) \tag{9.171}$$

$$\hat{R}_{k,m}^{p}(\tau) = \phi_{k,m}^{a}(\ell)\hat{R}_h(\delta) + \phi_{k,m}^{a}(\ell + 1)R_h(\delta) \tag{9.172}$$

where $\ell = \lfloor \tau/T_c \rfloor$ and $\delta = \tau - \ell T_c$. Note that δ is uniform on $[0, T_c)$ and ℓ is uniform on the set $\{0, 1, \ldots, N-1\}$. Combining (9.168), (9.171), and (9.172) gives

$$\begin{aligned} B_{k,1}(x_n^{(k)}, x_{n-1}^{(k)}, \tau_k) = &\left[x_{n-1}^{(k)}\phi_{k,1}^{a}(\ell_k - N) + x_n^{(k)}\phi_{k,1}^{a}(\ell_k)\right]\hat{R}_h(\delta_k) \\ &+\left[x_{n-1}^{(k)}\phi_{k,1}^{a}(\ell_k + 1 - N) + x_n^{(k)}\phi_{k,1}^{a}(\ell_k + 1)\right]R_h(\delta_k) \end{aligned} \tag{9.173}$$

To proceed any further requires information about the aperiodic cross-correlation functions of the spreading sequences being used, as well as the chip amplitude shaping function. One possibility is to assume random spreading sequences, where the length-N spreading sequences $\mathbf{a}^{(i)} = \{a_k^{(i)}\}_{k=1}^{N}$ are generated randomly such that the $a_k^{(i)}$ are randomly chosen from the set $\{-1, +1\}$ with equal probability. For random spreading sequences and a rectangular chip shaping function $h_c(t) = u_{T_c}(t)$, Morrow and Lehnert [230] have shown that

$$B_{k,1}(x_n^{(k)}, x_{n-1}^{(k)}, \tau_k) = x_{n-1}^{(k)}\frac{\delta_k}{N} + x_n^{(k)}\frac{(1-\delta_k)}{N} + \frac{X_k}{N} + \frac{Y_k}{N}(1 - 2\delta_k), \tag{9.174}$$

where δ_k is uniform on $[0, 1)$, $x_{n-1}^{(k)}$ and $x_n^{(k)}$ are uniform on $\{-1, +1\}$, and X_k and Y_k are discrete random variables having the probability distribution functions

$$p_{X_k}(i) = \frac{1}{2^{-A}}\binom{A}{\frac{i+A}{2}}, \quad i \in \{-A, -A+2, \ldots, A-2, A\} \tag{9.175}$$

$$p_{Y_k}(i) = \frac{1}{2^{-B}}\binom{B}{\frac{j+B}{2}}, \quad i \in \{-B, -B+2, \ldots, B-2, B\}. \tag{9.176}$$

The quantities A and B are related to

$$C \triangleq N\phi_{1,1}^{a}(1) = \sum_{j=0}^{N-2} a_j^{(1)} a_{j+1}^{(1)} \tag{9.177}$$

by

$$A = \frac{N-1+C}{2} \tag{9.178}$$

$$B = \frac{N-1-C}{2} \tag{9.179}$$

where $\phi_{1,1}^{a}(1)$ is the aperiodic cross-correlation of the spreading sequence of the first user. The parameter B is the number of chip boundaries in one period of the sequence $\mathbf{a}^{(1)}$ at which a transition to a different value occurs. For random spreading sequences, C has the probability distribution

$$p_C(i) = \frac{1}{2^{N-1}} \binom{N-1}{\frac{i+N-1}{2}}, \quad i \in \{-N+1, -N+3, \ldots, N-3, N-1\}. \tag{9.180}$$

9.6.1 Standard Gaussian Approximation

The standard Gaussian approximation assumes that the multiple-access interference

$$I = \sum_{k=2}^{K} B_{k,1}(x_n^{(k)}, x_{n-1}^{(k)}, \tau_k) \cos\phi_k \tag{9.181}$$

for sufficiently large K can be modeled as a Gaussian random variable with a distribution that is completely specified by its mean and variance. The approximation is obtained by conditioning the multiple-access interference on the random set of parameters $\{\delta_k, \phi_k, B \text{ or } C\}$ followed by ensemble averaging. Starting with the result in (9.174), it is straightforward to show that

$$\mathrm{E}[B_{k,1}(x_n^{(k)}, x_{n-1}^{(k)}, \tau_k)|C] = 0 \tag{9.182}$$

since the conditional density functions for $x_n^{(k)}$, $x_{n-1}^{(k)}$, X_k, and Y_k are symmetrical about zero. Hence, $\mathrm{E}[W_k] = 0$ and $\mathrm{E}[I] = 0$.

To compute the variance of the multiple-access interference, it is convenient to define the vectors $\boldsymbol{\delta} = (\delta_1, \delta_2, \ldots, \delta_K)$ and $\boldsymbol{\phi} = (\phi_1, \phi_2, \ldots, \phi_K)$. The variance of the multiple-access interference is

$$\begin{aligned}
\sigma_I^2 &= \mathrm{E}\left[I^2 \,|\boldsymbol{\delta}, \boldsymbol{\phi}, B\right] \\
&= \frac{1}{N^2} \sum_{k=2}^{K} \mathrm{E}\left[B_{k,1}^2(x_n^{(k)}, x_{n-1}^{(k)}, \tau_k)\,|\delta_k, B\right] \mathrm{E}\left[\cos^2\phi_k\,|\phi_k\right] \\
&= \frac{1}{2} \sum_{k=2}^{K} (1 + \cos(2\phi_k)) \mathrm{E}\left[B_{k,1}^2(x_n^{(k)}, x_{n-1}^{(k)}, \tau_k)\,|\delta_k, B\right]
\end{aligned} \tag{9.183}$$

Since all the Z_k are independent it follows that

$$\mathrm{E}\left[B_{k,1}^2(x_n^{(k)}, x_{n-1}^{(k)}, \tau_k)\,|\delta_k, B\right] = \frac{2(2B+1)(\delta_k^2 - \delta_k) + N}{N^2} \tag{9.184}$$

so that

$$\sigma_I^2 = \frac{1}{2}\sum_{k=2}^{K}(1+\cos(2\phi_k))\frac{2(2B+1)(\delta_k^2-\delta_k)+N}{N^2}. \tag{9.185}$$

If the intended sequence is known, then B is known. For random sequences $\mathrm{E}[B] = (N-1)/2$, and using this value for B

$$\sigma_I^2 = \frac{1}{N}\sum_{k=2}^{K}(1+\cos(2\phi_k))(\delta_k^2-\delta_k+1/2). \tag{9.186}$$

Several possibilities can be examined from here, including the following two important cases.

9.6.1.1 Chip and Phase Asynchronous Signals

The interfering signals are characterized by δ uniform on $[0,1)$ and ϕ uniform on $[0,2\pi)$ so that $\mathrm{E}[\delta_k^2-\delta_k] = -1/6$ and $\mathrm{E}[\cos(2\phi)] = 0$. In this case, $\sigma_I^2 = (K-1)/3N$. Hence, the decision variable in (9.167) can be interpreted as Gaussian random variable with mean $x_n^{(1)} \in \{-1,+1\}$ and variance $(K-1)/3N$ leading to the probability of bit error

$$P_b = Q\left(\sqrt{\frac{3N}{K-1}}\right). \tag{9.187}$$

The carrier to interference ratio C/I can be defined as the carrier power divided by the total noise power

$$\frac{C}{I} = \frac{1}{K-1}. \tag{9.188}$$

By comparing (9.187) with the probability of bit error for binary signaling on an AWGN channel, i.e., $P_b = Q(\sqrt{2\gamma_b})$ observe that the C/I and the effective bit energy-to-noise ratio, γ_b, are related by

$$\gamma_b = \frac{2N}{3}\frac{C}{I}. \tag{9.189}$$

9.6.1.2 Chip and Phase Synchronous Signals

The interfering signals have $\delta_k = 0$ and $\phi_k = 0$ so that $\sigma_I^2 = (K-1)/N$ and

$$P_b = Q\left(\sqrt{\frac{N}{K-1}}\right). \tag{9.190}$$

For chip and phase synchronous signals C/I and the effective γ_b are related by

$$\gamma_b = 2N\frac{C}{I}. \tag{9.191}$$

Coherent addition of interfering signals yields worst case interference with random spreading sequences. The orthogonal Walsh-Hadamard sequences are less random (secure) but yield zero correlation (better performance) under this condition.

9.6.2 Improved Gaussian Approximation

The standard Gaussian approximation can be quite inaccurate when the number of simultaneous users K is small or the processing gain N is large. To circumvent this deficiency a number of improved approximations have been developed.

A simple and more accurate Gaussian approximation has been derived by Holtzman [166]. To describe this method, let $P(\theta)$ be any function of a random variable θ having mean μ and variance σ^2. Then using a Taylor series expansion about the mean μ gives

$$P(\theta) = P(\mu) + (\theta - \mu)P'(\mu) + \frac{1}{2}(\theta - \mu)^2 P''(\mu) + \cdots \tag{9.192}$$

Taking expectations

$$\mathrm{E}[P(\theta)] \approx P(\mu) + \frac{1}{2}P''(\mu)\sigma^2. \tag{9.193}$$

Instead of using the Taylor series expansion, start instead with differences (Stirling's formula) and write

$$\begin{aligned} P(\theta) = P(\mu) &+ (\theta - \mu)\frac{P(\mu + h) - P(\mu - h)}{2h} \\ &+ \frac{1}{2}(\theta - \mu)^2 \frac{P(\mu + h) - 2P(\mu) + P(\mu - h)}{h^2} + \cdots \end{aligned} \tag{9.194}$$

Taking expectations

$$\mathrm{E}[P(\theta)] \approx P(\mu) + \frac{1}{2}\frac{P(\mu + h) - 2P(\mu) + P(\mu - h)}{h^2}\sigma^2. \tag{9.195}$$

Holtzman [166] has shown that $h = \sqrt{3}\sigma$ yields good results so that

$$\mathrm{E}[P(\theta)] \approx \frac{2}{3}P(\mu) + \frac{1}{6}P(\mu + \sqrt{3}\sigma) + \frac{1}{6}P(\mu - \sqrt{3}\sigma). \tag{9.196}$$

To apply the above result, let μ and σ^2 be the mean and variance of σ_I^2 in (9.185). It follows that

$$\mu = \frac{(K-1)}{N^2}\mathrm{E}[L_k]. \tag{9.197}$$

where

$$L_k = \frac{1}{2}(1 + \cos(2\phi_k))\left(2(2B+1)(\delta_k^2 - \delta_k) + N\right). \tag{9.198}$$

Then

$$\begin{aligned} \mu &= \frac{K-1}{N^2}\left(\frac{N}{2} - \frac{\mathrm{E}[B]}{3} - \frac{1}{6}\right) \\ &= (K-1)/3N \end{aligned} \tag{9.199}$$

where the last line assumes ensemble averaging with random spreading sequences. The variance is

$$\begin{aligned} \sigma^2 &= \frac{K-1}{N^4}\left(\mathrm{E}[L_k^2] - \mathrm{E}^2[L_k] + (K-2)\mathrm{cov}(L_j, L_k)\right) \quad \text{for any } j \neq k. \\ &= \frac{K-1}{N^4}\left(\frac{23}{360}N^2 + \left(\frac{1}{20} + \frac{K-2}{36}\right)N - \frac{1}{20} - \frac{K-2}{36}\right). \end{aligned} \tag{9.200}$$

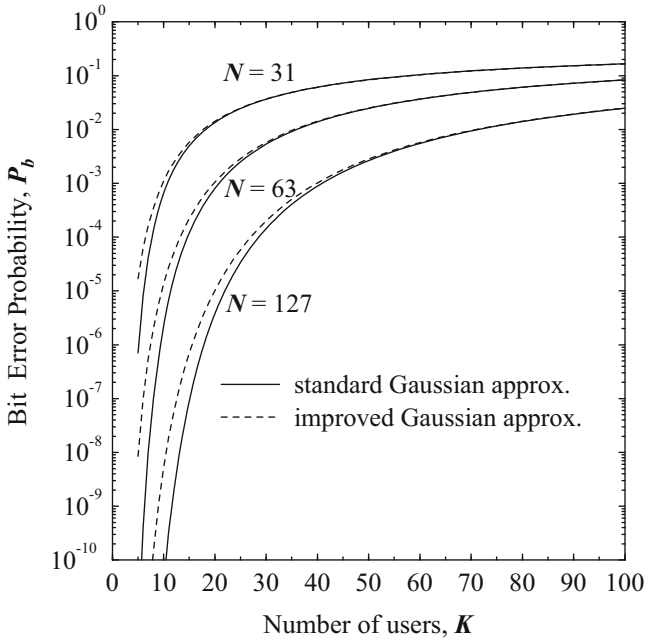

Fig. 9.30 Bit error probability against the number of users and various processing gains. The standard Gaussian approximation is shown to underestimate the error probability for small numbers of users

This yields

$$P_b \approx \frac{2}{3}Q\left(\sqrt{\frac{3N}{K-1}}\right) + \frac{1}{6}Q\left(\frac{1}{\sqrt{(K-1)/3N + \sqrt{3}\sigma}}\right) + \frac{1}{6}Q\left(\frac{1}{\sqrt{(K-1)/3N - \sqrt{3}\sigma}}\right). \tag{9.201}$$

The above calculations are very simple and lead to quite accurate results for all values of K and N. Figure 9.30 compares the standard and improved Gaussian approximations for various processing gains and number of simultaneous users. Note that the standard Gaussian approximation underestimates the error probability for small numbers of users. In this case, the improved Gaussian approximation should be used. However, the accuracy of the standard Gaussian approximation improves when the number of simultaneous users increases.

9.7 CDMA Multiuser Detection

The previous sections have considered the performance of DS CDMA with conventional correlation detection where the multiple-access interference was treated as an unwanted impairment that can have a detrimental affect on system performance. This section considers the use of CDMA multi-user detection to combat multiple-access interference. The concept of DS CDMA multi-user detection is very similar to the concept of co-channel demodulation discussed in Sect. 7.7. However, instead of distinguishing users by their different received pulses due to their signals propagation through different frequency-selective fading channels, DS CDMA multi-user detection distinguishes the different users by assigning them different spreading sequences. In any case, the mathematical development is very similar and results from Sect. 7.7 will be used in our treatment of CDMA multi-user detection.

Once again, consider a CDMA system consisting of K users that use short spreading codes. The transmitted complex envelope for the ith user is given by

$$\tilde{s}^{(i)}(t) = A\sum_{n=1}^{L} x_n^{(i)} a^{(i)}(t - nT), \tag{9.202}$$

where

$$a^{(i)}(t) = \sum_{k=0}^{N-1} a_k^{(i)} h_c(t - kT_c), \tag{9.203}$$

and $\mathbf{a}^{(i)} = \{a_0^{(i)}, \ldots, a_{N-1}^{(i)}\}$ and $\mathbf{x}^{(i)} = \{x_1^{(i)}, \ldots, x_L^{(i)}\}$ are the ith user's length-N spreading sequence and length-L data sequence, respectively. The data symbols $x_n^{(i)}$ are be independently chosen from the set $\{-1, +1\}$ with equal probability. The received complex envelope is given by

$$\tilde{r}(t) = A\sum_{i=1}^{K} g_i \tilde{s}^{(i)}(t - \tau_i) + \tilde{n}(t), \tag{9.204}$$

where the $\{g_i\}$, $g_i = \alpha_i e^{j\phi_i}$ and $\{\tau_i\}$ are the sets of random complex gains and delays that are introduced by the channel. The delays are assumed to assumed to satisfy the condition $0 \leq \tau_i \leq T$ for $1 \leq i \leq K$, where T is the data symbol duration. In the case of synchronous CDMA transmission, $\tau_i = 0$ for $1 \leq i \leq K$. Unlike the case of conventional correlation detection, the CDMA signals are not power controlled and may be received with different power levels due to the different channel gains α_i for $1 \leq i \leq K$. The fact that power control is not needed is a benefit of CDMA multi-user detection.

9.7.1 Optimum CDMA Multiuser Detection

The optimum CDMA multiuser detector determines the most likely sequence of transmitted bits $\mathbf{x}^{(i)} = \{x_1^{(i)}, \ldots, x_L^{(i)}\}$ for all users $1 \leq i \leq K$, given the observation of the received waveform $\tilde{r}(t)$. There are generally two cases to consider: synchronous CDMA and asynchronous CDMA. However, for our purpose only synchronous CDMA is considered where the received complex envelope is given by

$$\tilde{r}(t) = A\sum_{i=1}^{K} g_i \tilde{s}^{(i)}(t) + \tilde{n}(t). \tag{9.205}$$

In this case, it is sufficient to consider the received pulse corresponding to the kth baud interval, given by

$$\tilde{r}(t) = A\sum_{i=1}^{K} g_i x^{(i)} a^{(i)}(t) + \tilde{n}(t), \tag{9.206}$$

and to detect the corresponding data vector $\mathbf{x} = \{x^{(1)}, \ldots, x^{(K)}\}$. Similar to the development in Sect. 7.7, a complete set of complex orthonormal basis functions can be used to represent the received waveform $\tilde{r}(t)$ as a vector $\tilde{\mathbf{r}} = \{\tilde{r}_n\}$, such that

$$\tilde{r}_n = A\sum_{i=1}^{K} g_i x^{(i)} a_n^{(i)} + \tilde{n}_n, \tag{9.207}$$

where

$$a_n^{(i)} = \int_{-\infty}^{\infty} a^{(i)}(t)\varphi_n^*(t)\mathrm{d}t \tag{9.208}$$

$$\tilde{n}_n = \int_{-\infty}^{\infty} \tilde{n}(t)\varphi_n^*(t)\mathrm{d}t. \tag{9.209}$$

The $\tilde{n}_n$ are uncorrelated zero-mean complex Gaussian random variables with variance $\frac{1}{2}\mathrm{E}[|\tilde{n}_n|^2] = N_o$, so that the received vector $\tilde{\mathbf{r}}$ has the joint conditional multivariate Gaussian density

$$p(\tilde{\mathbf{r}}|\mathbf{x}) = \prod_{n=1}^{N} \frac{1}{2\pi N_o} \exp\left\{-\frac{1}{2N_o}\left|\tilde{r}_n - A\sum_{i=1}^{K} g_i x^{(i)} a_n^{(i)}\right|^2\right\}. \tag{9.210}$$

The optimum receiver chooses vector of symbols $\mathbf{x} = \{x^{(1)}, \ldots, x^{(K)}\}$ to maximize $p(\tilde{\mathbf{r}}|\mathbf{x})$ or, equivalently, to minimize the metric

$$\mu(\mathbf{x}) = \sum_{n=1}^{N}\left|\tilde{r}_n - A\sum_{i=1}^{K} g_i x^{(i)} a_n^{(i)}\right|^2. \tag{9.211}$$

Since $\sum_{n=1}^{N} |\tilde{r}_n|^2$ is independent of $\mathbf{x}$, maximizing (9.211) is equivalent to maximizing

$$\mu(\mathbf{x}) = 2\mathrm{Re}\left\{A\sum_{i=1}^{K} g_i^* x^{(i)*} \sum_{n=1}^{N} \tilde{r}_n a_n^{(i)*}\right\} - A^2 \sum_{i=1}^{K}\sum_{i'=1}^{K} g_i x^{(i)} g_i^* x^{(i')*} \sum_{n=1}^{N} a_n^{(i)} a_n^{(i')*}. \tag{9.212}$$

In the limit as the number of observable random variables N approaches infinity, define

$$y^{(i)} \triangleq \lim_{N\to\infty} \sum_{n=1}^{N} \tilde{r}_n a_n^{(i)*} = \int_{-\infty}^{\infty} \tilde{r}(t) a^{(i)*}(t)\mathrm{d}t \tag{9.213}$$

$$R_{i,i'} \triangleq \lim_{N\to\infty} \sum_{n=1}^{N} a_n^{(i)} a_n^{(i')*} = \int_{-\infty}^{\infty} a^{(i)}(t) a^{(i')*}(t)\mathrm{d}t. \tag{9.214}$$

Using (9.213) and (9.214) in (9.212) yields the final form

$$\mu(\mathbf{x}) = 2\mathrm{Re}\left\{A\sum_{i=1}^{K} g_i^* x^{(i)*} y^{(i)}\right\} - A^2 \sum_{i=1}^{K}\sum_{i'=1}^{K} g_i x^{(i)} g_i^* x^{(i')*} R_{i,i'}. \tag{9.215}$$

The variables $\{y^{(i)}\}$, $1 \le i \le K$ in (9.213) are obtained by passing the received complex envelope $\tilde{r}(t)$ through a bank of K correlators or matched filters and sampling the outputs. This essentially despreads and detects the received signal. The parameter $R_{i,i'}$ in (9.214) is equal to the full period cross-correlation between the spreading waveforms $a^{(i)}(t)$ and $a^{(i')}(t)$.

The decision metric in (9.215) can be put into a convenient vector product form as follows:

$$\mu(\mathbf{x}) = 2\mathrm{Re}\left\{\mathbf{x}^H \mathbf{G}^* \mathbf{y}\right\} - \mathbf{x}^H \mathbf{G}^* \mathbf{R} \mathbf{G} \mathbf{x}, \tag{9.216}$$

where

$$\mathbf{y} = (y^{(1)}, y^{(2)}, \ldots, y^{(K)})^T \tag{9.217}$$

$$\mathbf{x} = (x^{(1)}, x^{(2)}, \ldots, x^{(K)})^T \tag{9.218}$$

$$\mathbf{G} = \mathrm{diag}[Ag_1, Ag_2, \ldots, Ag_K] \tag{9.219}$$

$$\mathbf{R} = [R_{i,i'}]_{K\times K}, \tag{9.220}$$

and $\mathbf{x}^H$ is the complex conjugate transpose of $\mathbf{x}$. Note that the optimum detector must know or estimate the complex channel gains g_i, $1 \le i \le K$ to compute the decision metrics. The matrix $\mathbf{R}$ may be assumed known, since the spreading sequences are known. It is apparent that the complexity of the optimal detector grows exponentially with the number of users K and becomes impractical for large K. For this reason, a number of sub-optimum CDMA multi-user detectors have been suggested in the literature.

9.7.2 Decorrelating Detector

The vector of samples at the output of the K correlators or matched filters is

$$\mathbf{y} = \mathbf{GRx} + \boldsymbol{\nu}, \tag{9.221}$$

where the zero-mean Gaussian noise vector

$$\boldsymbol{\nu} = (\nu^{(1)}, \nu^{(2)}, \ldots, \nu^{(K)})^T \tag{9.222}$$

has covariance matrix

$$\boldsymbol{\Phi}_{\boldsymbol{\nu}\boldsymbol{\nu}} = \frac{1}{2}\mathrm{E}\left[\boldsymbol{\nu}\boldsymbol{\nu}^H\right] = N_o\mathbf{R}. \tag{9.223}$$

It follows that the vector $\mathbf{y}$ has a joint conditional complex Gaussian distribution with mean $\mathbf{GRx}$ and covariance matrix $N_o\mathbf{R}$. That is,

$$p(\mathbf{y}|\mathbf{x}) = \frac{1}{(2\pi N_o)^K|\mathbf{R}|^{1/2}}\exp\left\{-\frac{1}{2N_o}(\mathbf{y}-\mathbf{GRx})^H\mathbf{R}^{-1}(\mathbf{y}-\mathbf{GRx})\right\}. \tag{9.224}$$

The best linear estimate of $\mathbf{x}$ is the one that minimizes the metric

$$\mu(\mathbf{x}) = (\mathbf{y}-\mathbf{GRx})^H\mathbf{R}^{-1}(\mathbf{y}-\mathbf{GRx}) \tag{9.225}$$

which results in the solution

$$\tilde{\mathbf{x}} = \mathbf{R}^{-1}\mathbf{G}^{-1}\mathbf{y}. \tag{9.226}$$

To see how the decorrelator works, substitute (9.221) into (9.226) to obtain

$$\tilde{\mathbf{x}} = \mathbf{x} + \mathbf{R}^{-1}\mathbf{G}^{-1}\boldsymbol{\nu} \tag{9.227}$$

Finally, the binary symbol decisions are obtained by

$$\hat{\mathbf{x}} = \mathrm{sign}(\tilde{\mathbf{x}}). \tag{9.228}$$

Note that the decorrelator detector removes the multi-user interference in the signal terms, and this makes the detector near-far resistance so that power control is not necessary. Also, the decorrelator detector inverts the channel $\mathbf{G}$. This will result in noise enhancement for users that have small channel gains, g_i. Finally, if one or more pairs of spreading sequences are highly correlated, the matrix $\mathbf{R}$ is ill-conditioned and will also cause noise enhancement.

9.7.3 Minimum Mean Square Error Detector

The MMSE detector is one that chooses the linear solution $\tilde{\mathbf{x}} = \mathbf{Ay}$ to minimize the mean square error (MSE)

$$J(\mathbf{x}) = \frac{1}{2}\mathrm{E}_{\mathbf{x},\boldsymbol{\nu}}[\|\mathbf{x}-\tilde{\mathbf{x}}\|^2] = \frac{1}{2}\mathrm{E}[\|\mathbf{x}-\mathbf{Ay}\|^2], \tag{9.229}$$

where the expectation is over both the random data and noise vectors. The MMSE solution occurs when the error vector $\mathbf{x}-\mathbf{Ay}$ is orthogonal to the observation vector $\mathbf{y}$, i.e.,

$$\begin{aligned}\frac{1}{2}\mathrm{E}_{\mathbf{x},\boldsymbol{\nu}}[(\mathbf{x}-\mathbf{Ay})\mathbf{y}^H] &= \mathbf{0}\\ \frac{1}{2}\mathrm{E}_{\mathbf{x},\boldsymbol{\nu}}[\mathbf{x}\mathbf{y}^H] - \mathbf{A}\frac{1}{2}\mathrm{E}_{\mathbf{x},\boldsymbol{\nu}}[\mathbf{y}\mathbf{y}^H] &= \mathbf{0}.\end{aligned} \tag{9.230}$$

For the case of synchronous CDMA,

$$\frac{1}{2}\mathrm{E}_{\mathbf{x},\boldsymbol{\nu}}[\mathbf{x}\mathbf{y}^H] = \frac{1}{2}\mathrm{E}_{\mathbf{x}}[\mathbf{x}\mathbf{x}^H\mathbf{R}^H\mathbf{G}^*] + \frac{1}{2}\mathrm{E}_{\boldsymbol{\nu}}[\mathbf{x}\boldsymbol{\nu}^H] = \frac{1}{2}\mathbf{R}^H\mathbf{G}^* = \frac{1}{2}\mathbf{R}\mathbf{G}^*, \tag{9.231}$$

since $\mathrm{E}_{\mathbf{x}}[\mathbf{x}\mathbf{x}^H] = \mathbf{I}$ with uncorrelated data, the noise vector $\boldsymbol{\nu}$ has zero mean, and $\mathbf{R}$ is a Hermitian matrix, i.e., $\mathbf{R}^H = \mathbf{R}$. Also,

$$\begin{aligned}\frac{1}{2}\mathbf{A}\mathrm{E}_{\mathbf{x},\boldsymbol{\nu}}[\mathbf{y}\mathbf{y}^H] &= \frac{1}{2}\mathbf{A}\mathrm{E}_{\mathbf{x},\boldsymbol{\nu}}[(\mathbf{G}\mathbf{R}\mathbf{x}+\boldsymbol{\nu})(\mathbf{G}\mathbf{R}\mathbf{x}+\boldsymbol{\nu})^H] \\ &= \mathbf{A}\left(\frac{1}{2}\mathrm{E}_{\mathbf{x}}[\mathbf{G}\mathbf{R}\mathbf{x}\mathbf{x}^H\mathbf{R}^H\mathbf{G}^*] + \frac{1}{2}\mathrm{E}_{\boldsymbol{\nu}}[\boldsymbol{\nu}\boldsymbol{\nu}^H]\right) \\ &= \mathbf{A}\left(\frac{1}{2}\mathbf{G}\mathbf{R}\mathbf{R}^H\mathbf{G}^* + N_o\mathbf{R}\right) \\ &= \mathbf{A}\left(\frac{1}{2}\mathbf{G}\mathbf{R}\mathbf{R}\mathbf{G}^* + N_o\mathbf{R}\right).\end{aligned} \tag{9.232}$$

Substituting (9.231) and (9.232) into (9.230) and solving for $\mathbf{A}$ gives the equation

$$\frac{1}{2}\mathbf{R}\mathbf{G}^* - \mathbf{A}\left(\frac{1}{2}\mathbf{G}\mathbf{R}\mathbf{R}\mathbf{G}^* + N_o\mathbf{R}\right) = \mathbf{0} \tag{9.233}$$

which leads to the solution

$$\mathbf{A}_{\text{opt}} = \left[\mathbf{G}\mathbf{R} + 2N_o(\mathbf{G}^*)^{-1}\right]^{-1}. \tag{9.234}$$

Using $\mathbf{A}_{\text{opt}}$, the MMSE receiver computes the vector

$$\tilde{\mathbf{x}} = \mathbf{A}_{\text{opt}}\mathbf{y} \tag{9.235}$$

and makes the decisions

$$\hat{\mathbf{x}} = \text{sign}(\tilde{\mathbf{x}}). \tag{9.236}$$

Like the decorrelator detector, the MMSE detector is near-far resistant. Also, from (9.234), if the noise is negligible compared to the multi-user interference, i.e., $N_o = 0$, then $\mathbf{A}_{\text{opt}} = \mathbf{R}^{-1}\mathbf{G}^{-1}$ and the MMSE detector reduces to the decorrelator detector. On the other hand, if the noise is dominant compared to the multi-user interference, i.e., N_o is large, then from (9.234), $\mathbf{A}_{\text{opt}} = \mathbf{G}^*/2N_o$. In this case, the MMSE detector reduces to the conventional correlation detector.

Problems

9.1. Suppose that a DS/BPSK spread spectrum signal is corrupted by a single, phase-asynchronous, CW interfering tone at the carrier frequency. The received low-pass waveform is

$$\tilde{r}(t) = \tilde{s}(t) + \tilde{\imath}(t),$$

where $\tilde{s}(t)$ is defined in (9.4) and

$$\tilde{\imath}(t) = A_i e^{j\phi},$$

where ϕ is an arbitrary phase offset. Assume the use of a short Gold code (of arbitrary length). Compute the probability of bit error with a simple correlation detector.

9.2. Consider a DS/BPSK waveform that is subjected to broadband pulse jamming. In particular, a jammer with total power J jams the DS/BPSK waveform a fraction ρ of the time with additive white Gaussian noise having a two-sided power spectral density

$$\frac{N_J}{2\rho} = \frac{J}{2W_{ss}\rho},$$

where W_{ss} is the spread spectrum bandwidth, and $N_J = J/W_{ss}$ is the one-sided spectral density achieved by spreading the total jammer power J over the spread spectrum bandwidth W_{ss}. During the remaining fraction of time $1 - \rho$, the jammer is off and the received DS/BPSK waveform is assumed to be noise-free. It is assumed that each modulated and spread BPSK symbol is either completely jammed or not at all. The average received bit energy-to-jammer-noise ratio is defined as

$$\gamma_b = \frac{E_b}{N_J} = \frac{W_{ss}S}{R_bJ},$$

where S is the received desired signal power and R_b is the bit rate.

(a) Obtain an expression for the probability of bit error as a function of the jamming fraction ρ.
(b) Derive an expression for the jamming fraction ρ that will maximize the probability of bit error. Note that jamming fraction must satisfy the constraint $0 < \rho \leq 1$.
(c) What is the maximum bit error probability corresponding to the worst case jamming fraction found in part (b)?

9.3. Consider a non-coherently detected FH/BFSK waveform that is subjected to partial band noise jamming. In particular, a jammer with total power J jams a fraction ρ of the spread spectrum bandwidth W_{ss} with additive white Gaussian noise having a two-sided power spectral density

$$\frac{N_J}{2\rho} = \frac{J}{2W_{ss}\rho},$$

where $N_J = J/W_{ss}$ is the one-sided spectral density achieved by spreading the total jammer power J over the spread spectrum bandwidth W_{ss}. The remaining fraction $1 - \rho$ of bandwidth is free of jamming and is also assumed to be noise-free. It is assumed that each modulated and frequency hopped BFSK symbol is either completely jammed or not at all. The average received bit energy-to-jammer-noise ratio is defined as

$$\gamma_b = \frac{E_b}{N_J} = \frac{W_{ss}S}{R_bJ},$$

where S is the received desired signal power and R_b is the bit rate.

(a) Obtain an expression for the probability of bit error as a function of the jamming fraction ρ.
(b) Derive an expression for the jamming fraction ρ that will maximize the probability of bit error. Note that jamming fraction must satisfy the constraint $0 < \rho \leq 1$.
(c) What is the maximum bit error probability corresponding to the worst case jamming fraction found in part (b)?

9.4. The generator polynomials for constructing "Gold-like" code sequences of length $N = 7$ are

$$p_1(x) = 1 + x + x^3$$
$$p_2(x) = 1 + x^2 + x^3.$$

The sequences are said to be "Gold-like" because $p_1(x)$ and $p_2(x)$ are not a preferred pair and, therefore, will not actually generate a set of Gold sequences. However, the procedure used to construct the set sequences is similar to that used to construct Gold sequences. Generate all the "Gold-like" codes of length 7 and determine the cross-correlation functions of one sequence with each of the others.

9.5. Consider the length-7 m-sequences that are generated by the polynomials

$$p_1(x) = 1 + x + x^3$$
$$p_2(x) = 1 + x^2 + x^3.$$

(a) Find and sketch the full period autocorrelation functions of the sequences.
(b) Find and sketch the aperiodic autocorrelation function of the sequences.
(c) Find and sketch the full period cross-correlation function of the two sequences.
(d) Find the discrete-time Fourier transform of the aperiodic autocorrelation function, $\Phi^a(f)$, for each sequence.

9.6. Consider the length-7 Barker sequence

$$\mathbf{a} = (+1, +1, +1, -1, -1, +1, -1)$$

and its mirror image sequence

$$\mathbf{a} = (-1, +1, -1, -1, +1, +1, +1).$$

(a) Find and sketch the full period autocorrelation functions of the sequences.
(b) Find and sketch the aperiodic autocorrelation function of the sequences.
(c) Find and sketch the full period cross-correlation function of the two sequences.
(d) Sketch the discrete-time Fourier transform of the aperiodic autocorrelation function, $\Phi^a(f)$, and find the frequencies where it attains its maximum and minimum values.

9.7. Suppose that the following length-7 time-domain sequences are being proposed for the synchronization word in an OFDM system having block size $N = 7$.

$$\mathbf{x}_1 = (+1, +1, +1, -1, -1, +1, -1)$$
$$\mathbf{x}_2 = (+1, +1, +1, -1, +1, -1, -1)$$

(a) Compute and plot the periodic autocorrelation function and aperiodic autocorrelation function of these two sequences.
(b) Which sequence has better periodic autocorrelation characteristics for the purpose of synchronization.
(c) By taking the discrete-time Fourier transform of the aperiodic autocorrelation functions compute the power spectrum $\Phi^a(f)$ in each case. Plot your results.

9.8 (Computer Exercise). Write a computer program to generate a set of Gold sequences of length 127.

(a) Plot the mean and variance of the partial period autocorrelation as a function of the processing gain $10 \leq G \leq 20$ for this set of Gold codes.
(b) Repeat part (a) for the partial period cross-correlation.

9.9 (Computer Exercise). Consider a DS/BPSK CDMA system that uses length-31 Gold codes. The kth user spreads their binary data by using the Gold code

$$\mathbf{a}^{(k)} = (a_1^{(k)}, a_2^{(k)}, \ldots, a_{31}^{(k)}).$$

The complex envelope of the modulated waveform for the kth user is

$$\tilde{s}^k(t) = A \sum_n x_n^{(k)} h^{(k)}(t - nT),$$

where

$$h^{(k)}(t) = \sum_{j=1}^{31} a_j^{(k)} u_{T_c}(t - jT_c),$$

$\{x_n^{(k)}\}$ is uncorrelated zero-mean binary data sequence, T_c is the chip duration, and $T = 31T_c$ is the data bit duration.

(a) Pick one of the length-31 Gold codes at random for the kth user and write down the sequence. Plot the aperiodic autocorrelation function of sequence.
(b) Plot the power spectrum of the kth user $S_{\tilde{s}\tilde{s}}^{(k)}(f)$ against the normalized frequency fT_b.
(c) Repeat parts (a) and (b) for a randomly chosen length-63 Gold code for the kth user.

9.10. Plot the continuous-time partial autocorrelation functions of the chip waveform, $R_h(\delta)$ and $\hat{R}_h(\delta)$ in (9.32) and (9.33), respectively, as a function of the fractional chip delay δ for the following chip shaping pulses:

$$h_a(t) = \begin{cases} u_{T_c}(t) & \text{non-return-to-zero} \\ \sin(\pi t/T_c)u_{T_c}(t) & \text{half-sinusoid} \\ 1 - 2|t - T_c/2|/T_c u_{T_c}(t) & \text{triangular} \end{cases}$$

9.11. Consider the set of Walsh-Hadamard sequences of length 16. Determine full period autocorrelation $\phi_{k,k}(n)$ for this set of sequences. Tabulate your results in the $k \times n$ matrix

$$\boldsymbol{\rho} = [\rho_{k,n}]_{k\times n},$$

where $\rho_{k,n} = \phi_{k,k}(n)$.

9.12. A WLAN system uses biorthogonal modulation based on the use of length-8 Walsh-Hadamard codewords. Following the discussion leading to (4.81), a set of 16 biorthogonal signals is constructed according to

$$\begin{aligned} \tilde{s}_m(t) &= A\sum_{k=1}^{8} h_{m_k} h_c(t - kT_c)\ , && m = 1, \ldots, 8 \\ &= -\tilde{s}_m(t)\ , && m = 9, \ldots, 16, \end{aligned}$$

where T_c is the "chip duration" and $T = 8T_c$ is the symbol duration. Assume an uncorrelated data sequence and assume that all 16 signals are used with equal probability.

(a) Assuming that $h_c(t) = u_{T_c}(t)$, find the power density spectrum of the complex envelope $S_{\tilde{s}\tilde{s}}(f)$.
(b) Plot the power spectrum $S_{\tilde{s}\tilde{s}}(f)$ against the normalized frequency fT_b, where T_b is the *bit* duration.

9.13. A spread spectrum system transmits a binary data sequence $\mathbf{x} = \{x_k\}$, $x_i \in \{-1, +1\}$, by using the following length-3 short code spreading sequence

$$\mathbf{a} = (-1, +1, +1).$$

(a) Compute and plot the full period autocorrelation of the sequence **a**.
(b) Compute and plot the aperiodic autocorrelation of the sequence **a**.
(c) Suppose the chip shaping function is

$$h_a(t) = \sin\left(\frac{\pi t}{T_c}\right) u_{T_c}(t).$$

What is the transmitted power density spectrum $S_{\tilde{s}\tilde{s}}(f)$?
(d) At which frequencies is the receiver most sensitive to tone interference?

9.14 (Computer exercise). Consider the four length-15 spreading sequences identified in Example 9.1.

(a) Write a computer program to exhaustively search for and find the 4 sequences.
b) The periodic autocorrelation and cross-correlation of these sequences are also important to ensure rapid acquisition and to minimize multiuser interference. Define the 4×4 matrix $\Phi = [\phi_{k,k}]$, where $\phi_{k,k}$ is defined as the *maximum* off-peak periodic autocorrelation of sequence $\mathbf{x}^{(k)}$ and $\phi_{j,k}$ is the *maximum* cross-correlation between $\mathbf{x}^{(j)}$ and $\mathbf{x}^{(k)}$. These quantities are defined by

$$\phi_{j,k} = \max_n \left| \frac{1}{N} \sum_{i=1}^{N} x_i^{(k)} x_{i+n}^{(j)} \right|$$

Find the 4×4 matrix Φ.

9.15 (Computer Exercise). Suppose that a DS/BPSK spread spectrum system uses an m-sequence of length 127 as a long spreading code. The generator polynomial for the m-sequence is

$$p(x) = 1 + x^3 + x^7.$$

The processing gain G is equal to 10, i.e., there are 10 chips per modulated symbol.

(a) Assuming that $h_c(t) = u_{T_c}(t)$, find the power density spectrum of the complex envelope $S_{\tilde{s}\tilde{s}}(f)$. You must average over all possible subsequences of length 10.
(b) Plot the power spectrum $S_{\tilde{s}\tilde{s}}(f)$ against the normalized frequency fT_b, where T_b is the *bit* duration. Comment on the effect of using a long code on the power spectrum.

9.16. Suppose that the multipath intensity profile of a channel is given by

$$\phi_g(\tau) = \frac{P}{\mu_\tau} \mathrm{e}^{-\tau/\mu_\tau}.$$

(a) What is the average delay and delay spread of the channel?
(b) Suppose DS/BPSK spread spectrum is used on the channel. The receiver employs a two-tap RAKE receiver (assume ideal Nyquist pulses and maximal ratio combining). The tap spacing of the RAKE tapped delay line is equal to the chip duration T_c. Neglecting self-interference, write down an expression for the probability of bit error in terms of the average delay of the channel and the average received bit energy-to-noise ratio.
(c) If the bit error probability for a non-dispersive channel ($\mu_\tau = 0$) is 10^{-3}, what is the value of delay spread μ_τ that will reduce the bit error probability from 10^{-3} to 10^{-4}?

9.17. A multipath-fading channel has the multipath intensity profile

$$\phi_g(\tau) = \frac{P}{\mu_\tau} e^{-\tau/\mu_\tau}.$$

Suppose that DS/BPSK spread spectrum is used on this channel. The receiver employs a 3-tap, T_c-spaced, RAKE receiver with selective diversity combining. Assume ideal Nyquist pulses and the use of spreading sequences having an ideal autocorrelation function. Find the probability of error in terms of the average received bit energy-to-noise ratio.

9.18. Suppose that a 4-user synchronous CDMA system uses the following four length-15 spreading sequences:

$$\mathbf{x}_1 = \{-1-1-1-1-1+1+1-1-1+1+1-1+1-1+1\}$$
$$\mathbf{x}_2 = \{+1-1+1-1+1+1-1-1+1+1-1-1-1-1-1\}$$
$$\mathbf{x}_3 = \{-1-1-1+1+1+1-1+1+1+1-1+1+1-1+1\}$$
$$\mathbf{x}_4 = \{+1-1+1+1-1+1+1+1-1+1+1+1-1-1-1\}$$

Design a decorrelating detector, assuming an AWGN channel.